NASA Technical Memorandum 102621

Experimental Feasibility of Investigating Acoustic Waves in Couette Flow With Entropy and Pressure Gradients

Tony L. Parrott, William E. Zorumski, and John W. Rawls, Jr.

FEBRUARY 1990

National Aeronautics and
Space Administration

Langley Research Center
Hampton, Virginia 23665

TABLE OF CONTENTS

INTRODUCTION

The purpose of this paper is to assess the feasibility of an experimental program to study the effects of strong pressure, entropy and flow gradients on acoustic wave propagation in cylindrical Couette flow. The experimental design goal is to devise an experimental apparatus to control the entropy, pressure, and flow gradients in the annular region between independently rotating cylinders. Acoustic responses in this region are to be measured and correlated with theoretically predicted resonances, mode shape changes, or wave number shifts. The design and fabrication of an experimental apparatus to allow controlled superposition of the three gradients is a formidable challange to present technology; however, a conceptual approach to this complex experiment will be discussed along with intermediate experiments that can be done with current technology. A complicating requirement for an acoustic experiment with flow gradients is a flow regime amenable to analysis. Laminar Couette flow appears to be the simplest flow geometry for which this is possible.

Couette flow is produced in the annulus of two coaxial cylinders rotating at different spin rates. A large body of literature exists dealing with the stability of such flows. This early literature is summarized by Chandrasekhar [1], and a review of the literature up to 1980 is given by Di Prima and Swinney [2]. Near the end of the 19th centry, Mallock and Couette observed that the laminar flow between a rotating inner cylinder and a stationary outer cylinder became unstable as the speed of the inner cylinder was increased above a critical value. The two dimensional laminar flow was replaced by a three dimensional flow consisting of counter rotating vortices stacked one above the other in the axial direction. Later, G. I. Taylor [3] was able to predict analytically and also verify experimentally the speed where the Couette flow becomes unstable. Because of his work, these vortices and the speed where the flow becomes unstable are now associated with his name. Coles [4] investigation of the instabilities of Couette flow showed as many as 25 different flow states at a given rotational speed. More recently, Andereck et. al. [5] systematically varied the rotational speeds of the inner and outer cylinders and mapped a multitude of flow states as a function of Reynolds number. All of this work has been limited to incompressible flow.

The way in which transition to fully turbulent flow occurs is dependent upon which

cylinder has the higher rotational speed. If the speed of the inner cylinder is increased beyond the point where Taylor vortices initially appear, the flow structure remains regular but becomes increasingly complex. Many complex patterns are observed before the flow becomes fully turbulent. This process is referred to by Coles as transition by spectral evolution. Conversely, flows which are dominated by the rotation of the outer cylinder, transition to fully turbulent flow preceded by spiral bands of laminar and turbulent flow. In this case, transition occurs at a much higher rotational speed and with explosive suddenness. Coles refers to this transition process as catastrophic transition.

Snyder and Karlson [6] have studied experimentally the effects of a radial temperature gradient, or heat flux, and the stability of cylindrical Couette flow. A rotating inner cylinder and a fixed outer cylinder were used to show that a radial gradient, either inward or outward, has the initial effect of stabilizing the flow. The stability limit increases to a maximum value and then decreases as the gradient increases, and eventually becomes less than the constant-temperature limit.

The influence of a radial temperature gradient on the stability of Couette flow has drawn considerable attention, particularly by astrophysists and planetary scientists. Thermal convection in a rotating spherical shell is a basic model for the study of the convection process in stars and in the earth's core. Much has been learned about convection in spherical shells from the much simpler problem of rotating cylinders. The experimental study of Wimmer [7] demonstrates the close relationship between rotating spherical shells and rotating cylinders. His results indicate that Taylor's calculations for the onset of instability in rotating cylinders is also valid for rotating spheres.

An important first step in the proposed experimental program is to measure the effect of an isolated thermal gradient on acoustic wave propagation. The simplest experimental apparatus for accomplishing this is a rectangular waveguide with a thermal gradient imposed transverse to the longitudinal axis. The cavity would be excited in such manner and at frequencies such that selected cross modes would exist only in the direction of the thermal gradient. An analysis by Zorumski [8] indicated that the transverse temperature gradient should lower the resonant frequencies of longitudinal, nearly-plane, standing waves in the cavity.

The next stage of complication in the experimental program is to measure the effects of an isolated pressure gradient on acoustic propagation. This can be accomplished (in concept) by mounting the rectangular waveguide in a centrifuge such that the acceleration induces a transverse pressure gradient. Analysis by Zorumski [9] has indicated that the longitudinal resonant frequencies of the waveguide should be decreased by the pressure gradient. More importantly, low frequency resonances, related to buoyant oscillations, are predicted by the analysis. This physical experiment would be executed by an annulus rotating about a vertical axis—an analytically more complex situation than the accelerated waveguide. Predictions for this experiment, called the compressible Poincare problem, are given by Gans [10].

In rectangular Couette flow, or steady flow between sliding plates, the steady flow vorticity is constant and the Mach number is a linear function of the normal coordinate. Koutsoyannis [11] has given the acoustic waves for this case in terms of the Whittaker functions. This condition is approximated experimentally by the thin channel between slowly rotating cylinders of large radius.

Successive experiments would use combinations of the gradients. Pressure and entropy gradients may be combined with a rotating annulus which has either the inner or the outer cylinder heated to produce a radial heat flux. Pressure and velocity gradients are produced by adjusting the rotation speeds of the two cylinders which form the annulus. The average speed controls the pressure gradient, while the relative speed controls the radial velocity gradient. The final and ultimate apparatus for this research would allow the superposition of all three gradients of interest with some degree of independent control over each. The complex vortical flows that occur between rotating cylinders complicate the interpretation of strong gradient effects on acoustic propagation and should be avoided. The experiments would best be done in the stable laminar regime; however, if the flow is fully turbulent, it may still be possible to conduct meaningful acoustic experiments.

The following section presents some analysis to define more clearly the gradient parameters in the acoustic equations and some of the effects of these parameters on acoustic waves. This is followed by sections which define the design goals for the apparatus and some design details for the conceptual apparatus. These sections are followed by a discussion of

the instrumentation needed for the research. The paper concludes with recommendations for the development of a sequence of apparati for the study of the aeroacoustics of Couette flow.

SYMBOLS

a	acceleration vector, m/s^2
c	sound speed, m/s
c_p	specific heat at constant pressure, $J/kg \cdot K$
e	unit vector; ($\mathbf{e}_r$, $\mathbf{e}_\theta$)
f	frequency, Hz
g	acceleration due to gravity, m/s^2
i	$\sqrt{-1}$
k	wave number, m^{-1}
k_N	buoyant wave number, m^{-1}
L	length of circular cylinder, m
M	Mach number
$\bar{M}$	Average Mach Number
N	Väisälä-Brunt frequency, Hz
p	pressure, Pa
Q	source strength, s^{-1}
Q_r	radial heat flux, W
r	radius, m
r_c	critical radius, m
$\bar{r}$	average radius, m
R	gas constant , $N \cdot m/kg \cdot K$
Re	Reynolds number
s	entropy, $J/kg \cdot K$
T	temperature, K
$\bar{T}$	average temperature, K
t	time, s
u	velocity vector; (u_r, u_θ, u_z) , m/s
$\bar{u}$	average velovity, m/s
z	azmuthal coordinate, m

Greek:

γ	ratio of specific heats
η	radius ratio, r_1/r_2
θ	phase angle, rad
κ	thermal conductivity, $N/s \cdot K$
μ	absolute viscosity, $kg/m \cdot s$
ν	kinematic viscosity, m^2/s
ρ	density, kg/m^3
σ_{yield}	yield stress, Pa
ρ_m	plate density, kg/m^3
$\hat{\Phi}$	modified acoustic potential, m^2/s
$\hat{\chi}$	modified acoustic potential, m^2/s
$\hat{\Psi}$	acoustic potential, m^2/s
$\mathbf{\Omega}$	angular velocity vector $(\Omega_r, \Omega_\theta, \Omega_z)$, rad/s
ω	rotational frequency, rad/s

Superscripts:

~	unsteady
^	frequency transform
-	steady
'	spacial derivative

Subscripts:

l	mode shape in z direction
m	mode shape in y direction
n	mode shape in x direction
o	reference
r	radial component
θ	circumferential component
1	inner cylinder
2	outer cylinder

ANALYSIS OF GRADIENT EFFECTS

It was shown in references [8] and [9] that pressure and entropy are convenient thermodynamic state variables. This convention is continued here. The density and temperature are functions of the pressure and entropy. The equations are relatively simple for a perfect gas, and are given here for reference in the analysis which follows.

$$\rho = \rho_0 \left(\frac{p}{p_0}\right)^{1/\gamma} e^{-s/c_p} \tag{1}$$

$$T = T_0 \left(\frac{p}{p_0}\right)^{(\gamma-1)/\gamma} e^{s/c_p} \tag{2}$$

The logarithmic gradients of the density and temperature are linear functions of the logarithmic pressure gradient and the entropy gradient.

$$\frac{\nabla\rho}{\rho} = \frac{1}{\gamma}\frac{\nabla p}{p} - \frac{\nabla s}{c_p} \tag{3}$$

$$\frac{\nabla T}{T} = \frac{\gamma-1}{\gamma}\frac{\nabla p}{p} + \frac{\nabla s}{c_p} \tag{4}$$

General Acoustic Equations

In a system without flow, the steady momentum equation reduces to a balance between the acceleration and the pressure gradient.

$$\mathbf{\Omega} \times (\mathbf{\Omega} \times \mathbf{r}) + \mathbf{a} + \frac{\nabla p}{\rho} = \mathbf{0} \tag{5}$$

The acoustic pressure is defined in terms of a potential function $\tilde{\Psi}$.

$$\tilde{p} = \rho \frac{\partial \tilde{\Psi}}{\partial t} \tag{6}$$

The fluctuating velocity and acoustic potential are assumed to be time harmonic with frequency ω.

$$\tilde{\mathbf{u}} = \hat{\mathbf{u}} e^{-i\omega t} \tag{7}$$

$$\tilde{\Psi} = \hat{\Psi} e^{-i\omega t} \tag{8}$$

Combining the continuity and energy equations gives the following scalar equation relating the acoustic potential and the divergence of the acoustic velocity.

$$\nabla \cdot \hat{\mathbf{u}} + \frac{1}{c^2}\frac{\nabla p}{\rho} \cdot \hat{\mathbf{u}} - \frac{\omega^2}{c^2}\hat{\Psi} = \hat{Q} \tag{9}$$

The acoustic momentum equation is

$$\hat{\mathbf{u}} + \frac{2i}{\omega}\mathbf{\Omega} \times \hat{\mathbf{u}} + \frac{1}{\omega^2}\frac{\nabla p}{\rho}\frac{\nabla s}{c_p} \cdot \hat{\mathbf{u}} = -\nabla\hat{\Psi} + \frac{\nabla s}{c_p}\hat{\Psi} \tag{10}$$

The pressure and entropy gradients are variable coefficients in the acoustic equations and thus control the characteristics of acoustic waves. If other state variables such as density or temperature were used, the acoustic equations would appear to be more complicated, that is, the coefficients would be more complex expressions. It is apparent that significant simplifications result from having either the pressure or the entropy constant. The case of constant pressure with variable entropy (or temperature) was considered in reference [8] in the analysis of standing waves in a rectangular waveguide. When the temperature is constant, the entropy depends on the pressure so that the entropy gradient vector is opposite to the pressure gradient vector. This special case was considered in more detail in reference [9].

The wave equation is developed by eliminating the velocity components from equations (9) and (10). The dot product of the pressure and the entropy gradients appears when the momentum equation (10) is solved for the acoustic velocities. This product defines the Väisälä-Brunt frequency, which is a measure of the importance of the gradients.

$$N^2 = -\frac{\nabla p}{\rho} \cdot \frac{\nabla s}{c_p} \tag{11}$$

When N has a real value, the gas is statically stable. This means that a component of the entropy gradient must oppose the pressure gradient. This condition is satisfied, for example, in the case of constant temperature.

Constant pressure. When the pressure is constant, the temperature may be used as the thermodynamic state variable. The acoustic potential is defined in terms of a modified potential [8].

$$\hat{\Psi} = \sqrt{\frac{T}{T_0}}\hat{\Phi} \tag{12}$$

The homogeneous wave equation for $\hat{\Phi}$ contains the logarithmic temperature gradient.

$$\nabla^2\hat{\Phi} + \left(\frac{\omega^2}{c^2} + \frac{1}{4}\left|\frac{\nabla T}{T}\right|^2\right)\hat{\Phi} = 0 \tag{13}$$

The boundary conditions are also modified by the temperature gradient because the acoustic velocity depends on the gradient.

The natural frequencies of a rectangular waveguide such as shown in Fig. 1 depend on the gradient, or (equivalently) on the ratio of the temperature difference between the upper and lower walls to the average temperature in the waveguide. The formula for the natural frequencies has been developed to second-order accuracy.

$$\omega_{nml}^2 = \bar{\omega}_{nml}^2\left[1 + \alpha_{nml}\left(\frac{\Delta T}{\bar{T}}\right)^2\right] \tag{14}$$

The constant α_{nml} depends only on the constant-temperature standing wave numbers for the waveguide, namely $n\pi/L_x$, $m\pi/L_y$, and $l\pi/L_z$. The constant can be positive or negative, so that the temperature gradient may shift the resonant frequency either upward or downward. In the case of lowest-order modes normal to the gradient, (n,0,0), the frequency shift is downward. Further detail may be found in reference [8].

Constant temperature. If the temperature in the waveguide is constant, but the waveguide is accelerated in the z-direction, there will be a pressure gradient and an opposing entropy gradient. The Väisälä-Brunt frequency is real and (defined to be) positive. It was shown in reference [9] that the modified potential and homogeneous wave equation for this case are

$$\hat{\Psi} = exp\left[\frac{-p'}{2p}z\right]\hat{\Phi} \tag{15}$$

$$\left(\nabla_\perp^2 + \frac{\omega^2}{\omega^2 - N^2}\frac{\partial^2}{\partial z^2}\right)\hat{\Phi} + \frac{\omega^2}{c^2}\left(1 - \frac{(2-\gamma)^2}{4(\gamma-1)}\frac{N^2}{\omega^2 - N^2}\right)\hat{\Phi} = 0 \tag{16}$$

The above equation has constant coefficients and a separable solution for the rectangular waveguide. The dispersion equation is quadratic in ω^2 and has two positive solutions for the natural frequencies. Approximate solutions are as follows:

$$\omega_{nml1}^2 \approx \left(\frac{k_{ym}^2 + k_{zl}^2}{k_{xn}^2 + k_{ym}^2 + k_{zl}^2}\right) N^2 \tag{17}$$

$$\omega_{nml2}^2 \approx c^2\left(k_{xn}^2 + k_{ym}^2 + k_{zl}^2\right) + \left(\frac{(2-\gamma)^2}{4(\gamma-1)} + \frac{k_{xn}^2}{k_{xn}^2 + k_{ym}^2 + k_{zl}^2}\right) N^2 \tag{18}$$

The smaller natural frequency is proportional to the Väisälä-Brunt frequency and indicates a buoyant oscillation of the gas. The larger frequency is greater than the natural frequency of constant-pressure waveguide. Both frequencies depend on the Väisälä-Brunt frequency.

In this constant-temperature case, the Väisälä-Brunt frequency depends on the logarithmic pressure gradient. In a thin channel, the pressure gradient may be approximated by the ratio of the pressure differential to the channel heigth.

$$N \approx \frac{\sqrt{\gamma - 1}}{\gamma}\frac{c}{L_z}\left|\frac{\Delta p}{\bar{p}}\right| \tag{19}$$

The frequency shift due to a pressure gradient will then be positive and proportional to the logarithmic pressure difference across the channel $|\Delta p/\bar{p}|$.

Rotating Annulus

In a rotating annulus with a radial heat flux, the pressure and entropy are functions of radial position only. The acoustic momentum equations for the acoustic velocity components are then given by the following linear system.

$$\begin{bmatrix} \frac{\omega^2 - N^2}{\omega^2} & -2i\frac{\Omega_z}{\omega} & 0 \\ 2i\frac{\Omega_z}{\omega} & 1 & 0 \\ 0 & 0 & 1 \end{bmatrix} \begin{Bmatrix} \hat{u}_r \\ \hat{u}_\theta \\ \hat{u}_z \end{Bmatrix} = -\begin{Bmatrix} \frac{\partial \hat{\Psi}}{\partial r} \\ \frac{1}{r}\frac{\partial \hat{\Psi}}{\partial \theta} \\ \frac{\partial \hat{\Psi}}{\partial z} \end{Bmatrix} + \frac{s'}{c_p}\begin{Bmatrix} \hat{\Psi} \\ 0 \\ 0 \end{Bmatrix} \tag{20}$$

The determinant of the coefficient matrix above is zero when

$$N^2 = \omega^2 - 4\Omega_z^2 \tag{21}$$

Since the Väisälä-Brunt frequency will depend on radius, the radial positions where this determinant is zero are possible singular points of the wave equation for the acoustic potential. In the case of constant temperature, the Väisälä-Brunt frequency is proportional to radius.

$$N = \sqrt{\gamma - 1}\frac{\Omega_z^2}{c}r \tag{22}$$

There is then a single radius r_c where the equation is singular.

$$r_c = \frac{\sqrt{\omega^2 - 4\Omega_z^2}}{N'} \tag{23}$$

Note that N' is a constant for this constant-temperature case.

Assuming that the gas in the annulus is motionless, the temperature distribution is governed by

$$\nabla^2 T = 0 \tag{24}$$

but stability limits must be imposed to insure that the temperature distributions are possible in the experimental apparatus. Since the axis of the cylinder is to be vertical, the hydrostatic equation for the pressure gradient is

$$\frac{\nabla p}{\rho} = r\Omega_z^2 \mathbf{e}_r - g\mathbf{e}_z \tag{25}$$

The static stability limit then gives the following constraint on the temperature gradient

$$r\Omega_z^2\left(r\Omega_z^2 - c_p\frac{\partial T}{\partial r}\right) + g\left(g + c_p\frac{\partial T}{\partial z}\right) > 0 \tag{26}$$

The above condition is satisfied if the vertical and radial conditions are independently satisfied, that is, if

$$c_p\frac{\partial T}{\partial r} < r\Omega_z^2 \tag{27}$$

and

$$c_p\frac{\partial T}{\partial z} > -g \tag{28}$$

EXPERIMENTAL APPARATUS DESIGN GOALS

Several conceptual experiments were suggested in the Analysis section. The simplest of these would isolate the entropy gradient effect in a two-dimensional acoustic field established in a thin rectangular cavity. Cross-mode distortion and resonance frequency shifts would be studied by imposing a strong thermal gradient in the cross-mode direction. A more difficult experiment would isolate the pressure gradient effect by rotating an annulus on a vertical axis as shown in figure 2. The first of these experiments would validate predicted effects of entropy (or temperature) gradients in the absence of pressure gradients. The second experiment would do the same for pressure gradient effects. Combined effects of pressure and thermal gradients can be studied by incorporating heating and cooling mechanisms in the inner and outer cylinders. These experiments would avoid complicating effects of flow gradients. Upon successful completion of these experiments, a more elaborate experimental program would be undertaken to correlate theory and experiment for the combined flow, pressure, and entropy gradients.

The feasibility of constructing a concentric, rotating cylinder apparatus to allow independent control of all three gradients will be now be examined. A key requirement for the apparatus is that the annular region be terminated such that end effects are minimized in the test region. Because such boundary conditions will be difficult to achieve, it is advisable to proceed with a Phase I co-rotating cylinder apparatus that allows simultaneous control of pressure and thermal gradients but with no flow. This intermediate apparatus would not only provide experimental results of intrinsic value but would also provide valuable experience for refining the design of a Phase II apparatus. The Phase I experiments would proceed in parallel with the development of design solutions for critical aspects of the Phase II apparatus. Other than the independent spin rate capability and resulting instrumentation complications, Phase I and Phase II apparatus would be similar. The following subsection focuses on the conceptual design of the Phase I apparatus.

The pressure gradient in the rotating cylinder is controlled by the spin rate, which is proportional to the rotational velocity.

$$\frac{p'}{\rho c^2} = \frac{u_\theta^2}{rc^2} \tag{29}$$

The rotational velocity is limited by the strength of the rotating cylinder. Assuming that the hoop stress in the cylinder shell governs the design, the rotational velocity range is

$$0 \leq u_\theta < \sqrt{\frac{\sigma_{yield}}{\rho_m \, F.S.}} \tag{30}$$

Table I shows some physical properties of several metals. Titanium has the largest specific yield strength. Assuming a safety factor (F.S.) of 1.5 would give an upper limit on rotational velocity of about 424 m/s.

The rotational velocity is the product of radius and rotational speed Ω_z. A reasonable range for rotational speed is from zero to about 10,000 RPM.

$$0 \leq \Omega_z < 1047 \text{ rad/s} \tag{31}$$

The radius of the outer cylinder should then be about 400 mm.

$$r_2 = 400 \text{ mm} < \frac{424 \text{ m/sec}}{1047 \text{ rad sec}} \tag{32}$$

The gradients should be roughly radial for simplicity, although it may be convenient to have a slight vertical temperature gradient to insure stability. If the centrifugal acceleration is to dominate the gravititational acceleration, then

$$\frac{g}{r} << \Omega_z^2 \tag{31}$$

As mentioned previously, the Väisälä-Brunt frequency is a measure of the importance of combined gradients and of static stability. The buoyant wavenumber, which is the ratio of the Väisälä-Brunt frequency to the speed of sound, is an equivalent measure of the effects of gradients which has the advantage that the groups representing pressure and entropy gradients can both be expressed in dimensions of inverse length.

$$k_N^2 = \frac{N^2}{c^2} = -\frac{p'}{\rho c^2}\frac{s'}{c_p} \tag{34}$$

Curves of constant k_ν are shown in Fig. 3 with the pressure gradient as the abscissa and the entropy gradient as the ordinate. These curves are hyperbolas so that the points closest to the origin, for a given k_ν, are on the line with slope -1.

$$\frac{s'}{c_p} = -\frac{p'}{\rho c^2} \tag{35}$$

We use the design philosophy that the range of entropy gradients should be equivalent to the range of pressure gradients. This means that we should cover the square in Fig. 3 where the minimum entropy gradient is the negative of the maximum pressure gradient. The temperature gradient on the diagonal of this square is

$$\frac{T'}{T} = -(2-\gamma)\frac{p'}{\rho c^2} \tag{36}$$

The temperature gradient for a conductive temperature distribution is proportional to the net radial heat flux and inversely proportional to the radius.

$$T' = -\frac{Q_r}{2\pi\kappa L_z}\frac{1}{r} \tag{37}$$

Consequently, the range of heat flux depends on the properties of the gas in the annulus and the material selected for the cylinders.

$$0 \le \frac{Q_r}{L_z} \le 2\pi\frac{2-\gamma}{\gamma}\frac{\kappa}{R}\left(\frac{\sigma_{yield}}{\rho_m\, F.S.}\right) \tag{38}$$

Properties of some candidate gases are given in Table II. The heavy gas SF_6 may be useful in the Phase II experiments to provide supersonic Mach numbers. If this gas were used, the range of radial heat flux would be

$$0 \le \frac{Q_r}{L_z} \le 225 \text{ W/m} \tag{39}$$

The inner cylinder must be at a higher temperature than the outer to generate a positive heat flux. Since the conductive temperature profile is logarithmic,

$$0 \le T_1 - T_2 \le \frac{2-\gamma}{\gamma R}\left(\frac{\sigma_{yield}}{\rho_m\, F.S.}\right) ln\frac{r_2}{r_1} \tag{40}$$

Again using the combination of Titanium and Sulphur Hexaflouride, the difference in cylinder temperatures must be in the range

$$0 \le T_1 - T_2 \le 2535\, ln\frac{r_2}{r_1} \text{ K} \tag{41}$$

The annulus must be thin in order to keep the cylinder temperatures within a reasonable range. Thinness is also desirable for geometric simplicity, and it is helpful to select a radius ratio which will permit comparisons to other experiments. Many researchers [2] have used a value near 7/8 for the ratio r_1/r_2. This ratio would give $r_1 = 350$ mm and a temperature range of 340 K.

$$r_1 = 350 \text{ mm} \tag{42}$$

$$0 \leq T_1 - T_2 \leq 340 \text{ K} \tag{43}$$

Dynamic pressure sensors are currently available with a temperature range from 220 K to 545 K. With proper care on calibration, there is reason to believe that the lower temperature limit can be reduced slightly. For the present, it will be assumed that a lower temperature of 200 K can be achieved so that the temperature range will be

$$200\,\text{K} \leq T_2 \leq T_1 \leq 545\,\text{K} \tag{44}$$

When the temperature gradients are small the parameter $\Delta T/\bar{T}$ is approximately equal to $ln(T_2/T_1)$. Predictions are that a range from 0 to 1 for this parameter will produce strong temperature gradient effects. Similar results were found for pressure gradients with constant temperature. Consequently, a reasonable experimental goal is to vary the logarithms of the pressure and temperature ratios over the range (0, 1). The temperature range in equation (44) meets this goal.

$$ln\frac{T_1}{T_2} \leq ln\frac{545}{200} = 1.00 \tag{45}$$

It is convenient to fix the outer cylinder temperature at the lower temperature while varying the inner cylinder temperature.

$$T_2 = 200\,\text{K} \tag{46}$$

$$200\,\text{K} \leq T_1 \leq 545\,\text{K} \tag{47}$$

The pressure gradient equation (29) can be integrated to give the pressure ratio as a function of the cylinder temperatures and the spin rate.

$$ln\frac{p_2}{p_1} = ln\frac{r_2}{r_1}\frac{r_2^2\Omega^2}{R\,(T_1 - T_2)}e^{\zeta_2}\left[E_1(\zeta_2) - E_1(\zeta_1)\right] \tag{48}$$

$$\zeta(r) = 2\,ln\frac{r_2}{r_1}\frac{T(r)}{T_1 - T_2} \tag{49}$$

$$E_1(\zeta) = \int_\zeta^\infty \frac{e^{-t}}{t}\,dt \sim \frac{e^{-\zeta}}{\zeta} \tag{50}$$

At the maximum temperature difference, varying the spin rate will, according to equation (48) vary the pressure ratio over the range

$$0 \leq ln\frac{p_2}{p_1} \leq 1.03 \tag{51}$$

When the temperature difference between the cylinders is small, the asymtotic formula for the exponential integral E_1 gives a simple approximation for the pressure ratio.

$$ln\frac{p_2}{p_1} \sim \frac{1}{2}\frac{r_2^2\Omega^2}{RT_2} - \frac{1}{2}\frac{r_1^2\Omega^2}{RT_1}, \quad \frac{T_1 - T_2}{T_2} << 2\,ln\frac{r_2}{r_1} \tag{52}$$

In the case of constant temperature (200 K) variation of the spin rate over the complete range would produce an even larger range of pressure ratio.

$$0 \leq ln\frac{p_2}{p_1} \leq 1.80 \tag{53}$$

Alternatively, the pressure ratio range (0, 1) can be achieved with a lower spin rate range and higher uniform temperature. In any event, the complete range appears to be achievable for both temperature ratio and pressure ratio.

The range of entropy variation is readily found by integrating equation (4). The entropy at the inner cylinder will be equal to or greater than the entropy at the outer cylinder. The entropy range, based on the previous choices, would be

$$0 \leq \frac{s_1 - s_2}{c_p} \leq 1.10 \tag{54}$$

Phase II Apparatus

In the Phase II experiments, flow gradients will range from zero to the maximum attainable subject to mechanical and flow stability limitations. As indicated in the Introduction, a body of literature exists dealing with the stability of laminar Couette flow. Specifically, these analyses have dealt with the onset of laminar flow instabilities in relatively low speed flows of liquids (i.e incompressible flows).

Reynolds number range. Reynolds numbers $Re_1 = r_1\Omega_1^2/\nu$ and $Re_2 = r_2\Omega_2^2/\nu$ are used as parameters [1, 4, 5] when both cylinders are rotating. The sense of rotation is given usually by allowing the outer cylinder Reynolds number to be either positive or negative while restricting the inner cylinder Reynolds number to positive values. Fig. 4 shows a flow state diagram including both positive and negative values of Ω_1. Figure 4a shows the inviscid theory by Rayleigh, which predicts that the flow is stable if $0 < r_1^2\Omega_1 < r_2^2\Omega_2$ and $\Omega_2 > 0$. Figure 4b shows the viscous stability limits discovered by Taylor, plotted on a linear Reynolds number scale up to 10^4. The line $Re_1 = Re_2$ is the Rayleigh limit and the Taylor curve is asymptotic to this line for rotation in the same sense. The Taylor curve (for $\eta = 7/8$) crosses the ordinate at about $Re_1 = 10^3$ and increases slowly for $Re_2 < 0$. The limits are symmetric about the origin in the absence of gravity so the viscous effect makes the stability limit $Re_1 < 0$ for $Re_2 > 0$. A larger Reynolds number range is shown in Figure 4c, where the stability limits are plotted on a linear scale up to 10^5. Experiments and theory by Donnelly & Fultz indicate that $Re_1 \sim -|Re_2^{3/5}|$ if $Re_2 > 0$. On the other hand, experiments by Wendt (see Coles) and by Coles [4] indicate that the limit curve should cross the Re_2 axis between $Re_2 = 3 \times 10^4$ and $Re_2 = 10^5$. There remains a question of where the limit curve lies when Re_2 is large. Plotted on a linear scale of 10^6 as in Figure 4d, the Donnelly & Fultz theory would indicate that the lower limit curve is slightly below (but indistinguishable on this scale) the positive Re_2 axis. The experiments by Wendt and Coles are compressed into the origin on this scale, but they suggest that the limit curve may be above the Re_2 axis. The upper limit curve is presumably the Rayleigh line, but no experiments are available in this range, and the effect of compressibility is not included in the theories.

Since we are concerned with compressible flow and Reynolds numbers several orders of magnitude beyond those of previous studies, the definition of these limits must be part of our experimental investigation.

If the Phase II apparatus were operated at standard pressure, the Reynolds numbers would be enormous, on the order of 10^8. These numbers may be reduced by operating the apparatus at reduced gas pressures and densities. There are limits on the range of pressures,

however, which are derived from the acoustics of the experiments. The fluctuating pressure sensors can be expected to be sensitive down to about $10^{-6}p_0$ so that a practical lower limit for $\tilde{p}_{rms}$ is $10^{-5}p_0$. The upper limit on fluctuating pressure is the condition that pressure perturbations must be small in comparison to the static pressure within the cylinder. The lowest static pressure will be p_1 and, assuming a factor of 10^{-2} as a measure of smallness, the pressure range within the cylinder is defined.

$$10^{-5}p_0 \leq \tilde{p}_{rms} \leq 10^{-2}p_1 \tag{55}$$

$$10^{-3}p_0 \leq p_1 \tag{56}$$

Therefore, we can reduce the Reynolds numbers by three orders of magnitude by reducing the pressure within the annulus.

The manufacturer's data for SF_6 indicate that the viscosity is roughly proportional to temperature in our temperature range and can be represented by the following empirical formula.

$$\mu = \mu_0 \frac{T}{T_0} \tag{57}$$

Using previously-defined speed limits (0 to 1047 rad/s) and assuming $p_1 = 10^{-n}p_0$ gives a formula for the range of Re_1.

$$0 \leq Re_1 \leq 5.14 \times 10^{(7-n)} \left(\frac{T_0}{T_1}\right)^2 \tag{58}$$

A similar calculation, allowing for the higher pressure and speed at the outer cylinder, gives the range for Re_2.

$$0 \leq Re_2 \leq 6.71 \times 10^{(7-n)} \left(\frac{p_2}{p_1}\right) \left(\frac{T_0}{T_2}\right)^2 \tag{59}$$

The temperature ratio can be fixed, but the pressure ratio depends on both the cylinder temperatures and on the spin rates, that is, on both Re_1 and Re_2. This relationship is required to complete the definition of the Reynolds number range. The preceeding discussion has ignored the effect of temperature gradients on the stability limits. These effects must be considered with compressibility to properly define the range of possible Reynolds numbers. Recognizing the limitations of these unknowns, we will define the Mach number range below only for the case of constant temperature.

Mach number range. The mechanical limits on a plot with M_2 as the abscissa and M_1 as the ordinate are taken from equations (58) and (59).

$$M_1 \leq L_1 = \eta \left(\frac{r_2\Omega_{max}}{c_0}\right) \sqrt{\frac{T_0}{T_1}} = 2.71\sqrt{\frac{T_0}{T}} \tag{60}$$

$$M_2 \leq L_2 = \left(\frac{r_2\Omega_{max}}{c_0}\right)\sqrt{\frac{T_0}{T_2}} = 3.10\sqrt{\frac{T_0}{T}} \tag{61}$$

The inviscid stability limits are

$$0 \leq M_1 \leq \frac{1}{\eta}M_2 \tag{62}$$

Figure 5 shows the range of possible Mach numbers within the stability and speed limits for the case of constant temperature. The experimental region is enclosed by the connected line segments O-A-B-C-O.

It is not the Mach numbers themselves which are important for the contemplated acoustic experiments. Instead, the relative Mach number, or difference between the cylinder Mach numbers, and the pressure gradient, or pressure ratio, are the variables which must be controlled. It is intuitive that the average Mach number primarily controls the pressure ratio with a lesser effect due to the relative Mach number. We may show the range of pressure ratio by expressing this variable in terms of the average and relative Mach numbers. This may be done in the case of constant temperature by integrating the pressure gradient equation with the cylinders rotating at different speeds.

$$RTln\frac{p_2}{p_1} = \int_{r_1}^{r_2}\frac{u_\theta^2}{r}\,dr \tag{63}$$

The constant-viscosity laminar velocity profile is

$$u_\theta = Ar + \frac{B}{r} \tag{64}$$

where the constants A and B depend on the cylinder speeds. Using averages and differences of the cylinder speeds and radii as parameters gives a convenient form for the constants.

$$A = \frac{1}{2}\frac{\Delta r\bar{u} + \bar{r}\Delta u}{\bar{r}\Delta r} \tag{65}$$

$$B = \frac{r_1 r_2}{2}\frac{\Delta r\bar{u} - \bar{r}\Delta u}{\bar{r}\Delta r} \tag{66}$$

These expressions give the pressure ratio integral in terms of the average and relative Mach number parameters.

$$\frac{1}{\gamma}ln\frac{p_2}{p_1} = \left(\frac{\Delta M}{a}\right)^2 + \left(\frac{\bar{M}}{b}\right)^2 \tag{67}$$

$$\left(\frac{1}{a}\right)^2 = \frac{1}{2}\frac{\bar{r}}{\Delta r}\left[1 - \frac{r_1 r_2}{\bar{r}\Delta r}ln\frac{r_2}{r_1}\right] = \frac{1}{4}\frac{1+\eta}{1-\eta}\left[1 - \frac{\eta}{1+\eta^2}ln\,\eta^2\right] \tag{68}$$

$$\left(\frac{1}{b}\right)^2 = \frac{1}{2}\frac{\Delta r}{\bar{r}}\left[1 + \frac{r_1 r_2}{\bar{r}\Delta r}ln\frac{r_2}{r_1}\right] = \frac{1-\eta}{1+\eta}\left[1 + \frac{\eta}{1-\eta^2}ln\,\eta^2\right] \tag{69}$$

Equations(67-69) represent lines of constant pressure ratio as ellipses with major axes aligned with the relative Mach number ΔM and minor axes aligned with the average Mach number. The shape of the ellipse, that is a & b depends only on the radius ratio η. The size of the ellipse depends on the pressure ratio. In the present case, where $\eta = 7/8$,

$$a = 9.48261 \tag{70}$$

$$b = 2.74065 \tag{71}$$

Figure 6 shows the experimental region in terms of relative Mach number and pressure ratio. The boundary curves are parabolae in ΔM corresponding to the lines in Figure 5. If the temperature were 276.3 K, then point C would have a pressure ratio $ln\, p_2/p_1 = 1$. For all temperatures below this value, the relative Mach number may be varied between the stability limits while holding the pressure ratio constant.

$$\text{If} \quad T \leq 276.3 \quad \text{and if} \quad ln\frac{p_2}{p_1} \leq 1.0 \tag{72}$$

$$\text{Then} \quad -0.365\sqrt{\frac{1}{\gamma} ln\frac{p_2}{p_1}} \leq \Delta M \leq 4.74\sqrt{\frac{1}{\gamma} ln\frac{p_2}{p_1}} \tag{73}$$

The Reynolds number range may now be completely defined for the case of constant temperature, using the following sequence.

$$\bar{M} = b\sqrt{\frac{1}{\gamma} ln\frac{p_2}{p_1} - \left(\frac{\Delta M}{a}\right)^2} \tag{74}$$

$$M_1 = \bar{M} - \frac{\Delta M}{2} \tag{75}$$

$$M_2 = \bar{M} + \frac{\Delta M}{2} \tag{76}$$

$$Re_1 = 2.16 \times 10^{(7-n)} \eta \left(\frac{T_0}{T}\right)^{3/2} M_1 \tag{77}$$

$$Re_2 = 2.16 \times 10^{(7-n)} \left(\frac{T_0}{T}\right)^{3/2} \left(\frac{p_2}{p_1}\right) M_2 \tag{78}$$

End effects. The finite length of the cylinders must be considered in the design of the Phase II apparatus. Ideally, the angular velocity of the gas would be a function of radius only, simulating the infinite cylinder. This simulation is usually attempted by making the aspect ratio of the annulus, the length divided by the gap width, large. However, experiments by Coles and Van Atta [12] have shown that the ends have a large effect on

the mid-plane velocity profile even if the cylinder is long. Figure 7 illustrates this effect. In the experiments by Coles and Van Atta, the end plated were attached to the outer cylinder, and the aspect ratio of the annular gap was 27.35. The fluid at the end of the cylinder has the constant angular velocity of the end plate, whereas the velocity at the midplane varies between the inner and outer cylinders. The infinite cylinder velocity profile is nearly linear if the gap width is small compared to the cylinder radius, however the data showed that the midplane profile "moved toward" the end-plate profile by a significant amount. The actual angular velocity profile in this experiment is then a function of both radius and axial distance, that is, $\Omega = \Omega(r, z)$. The Phase II apparatus should be designed to minimize these end effects, making the angular velocity profile approach the infinite cylinder profile. Two approaches to this goal are mechanical design and boundary layer control.

Figure 8 illustrates the mechanical design approach. If half of the end plate is attached to the inner cylinder, and the other half attached to the outer, the angular velocity at the end will be discontinuous midway between the plates as shown in Figure 8a. The angular velocity at the mid-plane would then be expected to approximate the dashed line in Figure 8. If a central segment with angular velocity $\bar{\Omega}$ is inserted, the end-plate velocity profile would have two steps as shown in Figure 8b, and the mid-plane profile would be smoothed further. Multiple segments, as shown in Figure 8c, would bring the velocity profiles closer to the idealized curve.

The alternative to segmented end plates, which will be difficult to develop, is boundary layer control. Presumably, the end effect observed at the mid-plane is the result of diffusion of the end-plate boundary layer toward the central plane of the annulus. If suction is applied at the ends, there should be a tendendy to limit the outward diffusion of this boundary layer and thus bring the velocity profile into closer conformance with the infinite-cylinder profile. More detailed studies will be required to select the actual method of controlling end effects.

Hardware development phases. A feasible mechanical design configuration for a coaxial spinning cylinder apparatus gradients will depend upon material stress limits, rotational stability criteria, and ancillary systems to provide differential spin rates, thermal flux, acoustic inputs, and data acquisition. The thermal flux for entropy gradient production can be obtained by heating one cylinder and cooling the other. Thus the physical mechanisms for achieving a degree of independent control for all three gradients of interest can be identified; however, the detailed design considerations to insure a meaningful comparison of experiment with theory presents a formidable challenge. One of the greatest challenges is attaining an appropriate boundary condition at the annular region axial terminations. This boundary condition should ideally leave the Couette flow unperturbed.

Other design challenges involve the design of a distributed source to excite preferred modes and the design of traversing probes to measure both the aerothermal and acoustic fields in the annulus. All the systems must be packaged so that no significant interference with the aero-acoustic field occurs. Power requirements will be met with generators integrated with the central axle to avoid the use of slip rings.

Independent control of cylinder spin rates will provide a broad range of experimental conditions involving combinations of pressure and flow gradients. The addition of entropy gradients will greatly extend the possibilites. Because of the mechanical complexity attendant to independent control of cylinder spin rates and the implementation of an appropriate boundary condition at the test region axial terminations, it is preferable to evolve the experimental program through at least two phases as indicated previously. Because experimental conditions achievable with a phase I apparatus are a subset of those achievable with a phase II appartus, the two apparati should share several design features. Hardware development for the phase II boundary condition can proceed in parallel with the phase I experiment and, hopefully, be implemented in a timely manner at the completion of phase I.

MECHANICAL DESIGN FEATURES AND TRADEOFFS

Test Medium

As was suggested in the previous section, a test medium with a high molecular weight relative to that of air, and thus lower sound speed, will permit a higher cylinder surface Mach number to be attained for a given spin rate and cylinder radius. A heavy gas test medium will therefore allow a reduction in apparatus diameter and spin rate for a given relative velocity between the two cylinders. This scale reduction will be of great benefit in simplifying the mechanical and utility requirements.

Candidates for a heavy gas test medium must be nontoxic, environmentally benign, have well documented thermodynamic properties, and obey the perfect gas law over the pressure and temperature ranges of interest. At room temperature and atmospheric pressure, sulfur hexaflouride (chemical formula, SF_6) is a colorless, odorless, tasteless gas that is nonflammable and is completely nontoxic. At standard temperature and pressure, it has a density of $6.2\,kg/m^3$ and a sound speed of $136\,m/sec$. Other properties of interest are given in table I along with those for air and Freon-12 for comparison.

The applicable range of the perfect gas law encompases the pressure and temperature ranges of interest in this experiment by a wide margin. The gas is most commonly used in the electrical equipment industry because of its chemical stability and dielectric strength. These characteristics are of interest in this experiment should the need arise for a pulse type acoustic source driven by electrical discharges. Sulfur hexaflouride is commercially available and is shipped in steel cylinders as a liquified gas under its own vapor pressure of 23 atm and at a temperature of 21 °C.

Entropy Gradient Generation

In both phase I and phase II experiments, a controlled entropy gradient is generated in the annulus by imposing a thermal gradient across the annulus with an associated heat transfer. There are five ways to accomplish such a heat transfer as follows:

1) Convective heat transfer by exposing cylinder surfaces to hot or cold gas flows

2) Evaporative cooling by water droplet impingement on the appropriate cylinder surface

3) Resistive heating by embedded heating elements in cylinder and supplied with electrical power through slip rings

4) Radiant heat supplied by circumferentially spaced infrared heat lamps

5) Electric induction heating via solenoid coil located external to and coaxial with cylinder axes

Available technology, mechanical convenience, and controllability suggest that heat transfer to a rotating cylinder can most easily be accomplished by electric induction. Inductive heating occurs when a conductor is placed in a varying magnetic field. Thermal energy production results mainly from resistive heating caused by electric currents driven by induced eletromotive forces. Inside a conductor, the electromotive force is proportional to the time rate of change of magnetic flux. Thus if two thin walled cylinders of different magnetic permeabilities are enclosed by a solenoid carrying a high frequency current, then the cylinders will be heated in proportion to their respective permeabilities. Induced currents will tend to circulate in the circumferential direction around the cylinders. If the cylinders are allowed to rotate, additional electromotive forces are induced that tend to circulate currents in the radial direction. For thin walled cylinders, heat developed by these radial currents should be minimal except possibly at very high spin rates. Therefore the rate of inductive heating should be proportional to the inductive current.

The above considerations suggest that a thermal gradient can be maintained across the annulus between two rotating cylinders by a combination of differential inductive heating and evaporative cooling, at least at relatively low differential spin rates. If, for example, the inner and outer cylinder consist of a ferromagnetic and nonferromagnetic material respectively, with a permeability ratio of 5000:1, typical of that between steel and aluminum (see table II), then a large differential thermal energy input to each cylinder will exist provided that the temperature of the ferromagnetic material is maintained below its Curie temperature [14]. At the Curie temperature, the permeability of a ferromagnetic material tends toward 1. To maintain a constant thermal gradient, the outer cylinder will need to be evaporatively cooled by a water droplet spray. The chief advantages of this technique are the mechanical simplicity and heating uniformity. The disadvantage is the low tensile strengths of specialized ferromagnetic alloys, and the permeability decrease as the Curie temperature is approached.

Table II lists the relevant properties of several materials suitable for constructing cylinders that can be differentially heated by electric induction. It is of interest to note that a specialized magnetic alloy called Supermendur has a permeability of 13 times that of typical steel and a Curie temperature of 980 °C compared with 720 °C for steel. However, these materials are not intended to carry high stress loads that would be encountered in this application. To achieve the highest possible 'hot' cylinder temperature and spin rates, a composite cylinder would be needed consisting of an outer layer of a high strength material such as titanium around an inner layer of a ferromagnetic alloy such as Supermendur.

The technology for induction heating is well established and is used for precision heat treatments in metalurgy [13]. Commercial power supplies and control systems should

therefore be available. Power and cooling requirements can be specified once the scale of the experimental apparatus is determined.

Hardware Configuration

Because of power requirements, the cost of precision milling and safety concerns, it is preferable to keep the scale of the apparatus as small as possible. The central axle and inner cylinder must carry all instrumentation and ancillary systems. A convenient annulus width (boundary layer thickness) is 25 mm. An outer cylinder radius of 0.5 m should allow adequate space for the inner cylinder and ancillary systems. A central axle radius of 0.15 m should be sufficient to accomodate test medium supply lines, instrumentation, probe drives and power generators.

A low test medium density can be obtained by placing the entire rotating system in a controlled low pressure environment. Such an environment will lower the boiling point of the water used to maintain the cool cylinder temperature. Reduced pressures will also affect the design of the cylinder ring bearing system. These issues will be discussed in the section addressing the gas lubricated bearing design concept. Clearly, the estimates given above suggest that the prospect of attaining a relative cylinder Mach number near 2.4 and a unidirectional entropy gradient will require substantial engineering development.

A conceptual design overview of the proposed apparatus is illustrated in the vertical cross section sketch of figure (9). The sketch is generic in nature and applies to either a phase I or phase II apparatus. The central axle is supported by gas lubricated, thrust and journal bearings at bottom and top respectively. Phase I and II can probably share the same physical size, central axle support, and motor drive. Instrumentation and ancillary systems will be contained in the central axle with sensor probes extending radially into the annulus. To obtain detailed aerothermal data and acoustic mode structure information, the instrumentation for phase II will be more extensive and complex than for the phase I experiment.

The addition of independent cylinder spin rate control along with the requirement for supersonic flow speeds complicates the phase II design. In addition to the more complex instrumentation required, the bearing system that supports and constrains relative motion of the two cylinders must meet special reqirements. Ideally, the terminating boundary condition at either end of the annular test region should not alter the Couette flow. As discussed previously, such a flow boundary condition can be approximated by a 'stepped' bearing consisting of concentric rings. In the present concept for a phase II experiment, the multiple concentric rings are isolated from all metal contact by a high pressure gas film. (Evaporation of a liquid lubricant would contaminate the test medium.) The gas would

be the same as that for the test medium and the leakage from the bearings would provide the supply for the test region. The proposed concept for the multi-ring, gas lubricated, bearing system will be discussed further in a later section.

Inner cylinder rotation can be conveniently implemented with electric motors. Synchronous electric motors are available up to 18,000 RPM and horsepower ratings of up to 600. For the outer cylinder, impulse reaction jets symmetrically spaced around the axis to mimimize side thrusts on the bearing system may be preferable.

The entire apparatus is enclosed in an air-tight, explosion proof cylindrical container with an exhaust vent to a vacuum source. Evaporative cooling for the outer cylinder is provided by a water spray emanating from nozzles installed in the containment cylinder. The coolant, in the form of steam, exits the system through the exhaust ports to a vacuum source. (not shown). All construction materials are selected with due regard to heating from stray induction fields.

The only means to access the annular test region for the installation of acoustic sources and measurement instrumentation is via the central axle. Transversing probes at various locations will be required to measure velocities, temperatures, turbulence levels and acoustic pressures. All signal conditioning is contained in the central axle along with probe positioning mechanisms. Probe position control and data signal transmissions are implemented by telemetry. Conceptual schemes for accomplishing these tasks will be discussed in a subsequent section.

INSTRUMENTATION SYSTEMS

Acoustic Source Design and Installation

Excitation of controlled acoustic modes by means of distributed sources in the annular region is a critical aspect of the apparatus design. Ideally, it is desireable to set up a preselected mode in the annular region similar to the 'spinning' mode synthesizer developed for duct liner performance studies. For example, a zero order radial mode could be excited with a circumferential distribution of in-phase sources on the inner cylinder wall as dipected in the schematic of figure 9. A first order radial mode would require two arrays of circumferentially distributed, out-of-phase sources, located on opposite sides of the annulus. Each array is coupled to a single acoustic driver located in the central axle. Clearly, excitation of a first order radial mode in the annulus entails a complex mechanical arrangement. Thermal gradients in the waveguides, density gradients across the annular test region, and low absolute densities will complicate implementation. It would be particularly difficult to generate a first order radial mode in a phase II experiment. This could, in principle, be done with phased heat release produced by laser beams focused on opposite surfaces of the annulus. The lasers would be contained in the central axle with beam transmission through windows in the central axle and inner cylinder. Controlled radial mode orders beyond the first are not feasible for either phase I or phase II experiments as presently conceived.

A much simpler alternative source arrangement would use a pulse type excitation driven by an electrical discharge. This point-like source would be optimally located in the annulus such that reflected waves could be 'edited' out of the acoustic pressure time history. Alternatively, cepstrum analysis techniques could be exploited to 'window out' reflections. Initial studies could proceed with such a source while a more complex mode type source is under development. Disadvantages of the pulse source are limited ability to control the pressure spectrum, possible nonlinear propagation near the source and requirement for high voltage.

Measurement Instrumentation

Aeroacoustic measurements will be needed to define both the mean and fluctuating quantities. Temperature and velocity measurements will define the gradients across the annular region. These measurements must be performed by probes that can be radially traversed in the annular region. For the phase II apparatus with outer cylinder rotation, all measurement instrumentation must be built into the inner rotating cylinder system with the central axle serving as the support base. Radial probe traversing within the annulus can

be accomplished by a stepper motor arrangement located in the central axle, as indicated in figure 6. Likewise, fluctuating quantities will be obtained by radially traversing probes.

Figure 10 shows a conceptual design for a stepper motor driven probe system. The system as shown allows all probes to be mechanically synchronized by a multiple cam and follower arrangements sharing a common drive. The cams are driven by a specially designed stepper motor. Each multi-lobed cam would precisely locate several probes in the same axial plane as it rotates in a stepwise manner relative to the central axle. The probes, acting as cam followers, are spring loaded to compensate for centrifugal forces. The stepper motor design for this application is a single direction DC motor. An electromagnetic escapement actuated by a switched DC signal allows the output of the motor to be transformed into a stepped rotation of the cams, allowing precision controlled movements of the probes. Power for the motor and escapement is derived from a DC generator built into the axle. This in-situ generator would also supply power for various signal conditioning systems.

Acoustic probe design considerations. Meaningful comparisons of theory with experiment will require both amplitude and phase measurements. This implies a knowledge of the acoustic probe transfer function in the presence of flow and thermal gradients. Thus the development of probes that can be pre-calibrated before installation and for which environment dependent corrections can be reliably calculated will be needed. Alternatively, it may be possible to develop probes whose responses do not change significantly with the anticipated experimental conditions. The choice of design concepts will depend upon the availablity of sensors that can tolerate the anticipated temperatures. Two design concepts are considered here.

Figure (11) shows schematic diagrams illustrating two possible design concepts for acoustic pressure probes. Part (a) of the figure shows a concept in which the sensor is remotely located relative to the probe section exposed to high temperatures. This design emphasizes sensor survivability at the expense of complicating the probe response. The probe response function will be affected by thermal gradients between the ports and sensor diaphram unless provision is made for cooling. One cooling technique is to purge the probe with the test medium gas which would exit the probe ports. An alternate possibility is to locate the sensor very near the probe ports as indicated in part (b) of the figure. This design effectively moves the resonant response away from the frequency range of interest; however, sensor cooling by gas purging would then be mandatory for presently availabe pressure sensors. New fiber optic sensor technology may be sufficiently developed to exploit in the phase II experiment in which case some of the concerns for sensor survival may be alleviated.

Aerothermal measurements. Aerodynamic measurements can be obtained with con-

ventional pitot-static probes traversed across the annular region. Likewise, temperature measurements can be obtained with thermocouple probes. Several fixed point temperature measurements will likely be required on the cylinder walls to monitor overall heating and cooling processes. These measurements can be obtained with noncontacting, infrared sensors. The sensors for the inner cylinder can be located in the central axle and would 'look' at the inner cylinder surface through a transparent window built into the central axle surface. Outer cylinder temperature can be monitored by infrared sensors looking at the outside cylinder surface insulation.

Turbulence intensity measurements may also be required for the phase II experiment. These can be obtained with hot film probes traversed across the annular region by the cam follower arrangement. Hot films are probably the most fragile transducer element anticipated for use in the experiments and normally require frequent calibration. Instrumentation accessibility for maintenance and calibration is an important issue that has not been resolved for either a phase I or phase II experiment. One possibility is to provide enough redundancy to insure adequate data acquisition in the event of several transducer failures. Perhaps the only calibrations that can be performed will be done during pre- and post- appratus assembly phases. If such is the case, a sufficient amount of probe sensor development and testing will be required to to provide the necessary confidence levels.

Power Source and Signal Acquisition

Special efforts will be required to minimize power requrements for all ancillary systems in the central axle. It is anticipated that high torque motors may be required to rotate the probe actuating cam system which must drive the probes against the spring loadings required to offset the centrifugal loads at high rotational speeds. To insure the reliability of the power source and to avoid the mechanical inconvenience of slip rings, a DC power generator incorporated into the central axle will be necessary. Recharageable batteries could serve as the primary power source for stepper motors and instrumentation power supplies. The DC power generator armature could be integrated into the central axle with the field coil mounted stationary and concentric with the central axle. Telemetry linked data acquisition systems will be required for all aeroacoustic measurements.

PHASE II APPARATUS BEARING SYSTEM

This section discusses a unique feature of the phase II apparatus needed to mimimize distortion of the Couette flow profile near the ends of the two rotating cylinders of a phase II type apparatus. As discussed previously, the linear velocity profile can be approximated by step changes in the velocity profile at the end termination planes. This boundary condition will be the chief difference between the phase I and phase II apparatus. Also, at the high rotational speeds expected, it is critical that cylinder wall out-of-roundness be kept to an absolute minimum. This condition must be maintained for at least two reasons. First, small oscillatory changes in the test region width relative to the laboratory reference frame may be manifested as a strong pressure fluctuations at frequencies associated with the differential spin rate. Such pressure fluctuations could very well mask the much weaker source pressures. Secondly, any cylinder out-of-roundness or wall waviness will reduce the near-wall, spatial resolution for aerothermal measurements. An additional source of annular width variation will be associated with bearing eccentricities. One way to minimize these effects is to use hydrostatically, gas lubricated bearings. According to reference [16] the technology is available to implement such a system for a simple journal type bearing. In principle, the concept can be extended to a multi-ring bearing system appropriate for annular region termination between the two rotating cylinders.

The basic concept for a multi-ring gas lubricated bearing system is described with the help of figure (12). The figure shows a magnified cross section of the bottom termination of the annular region between the two concentric rotating cylinders illustrated in figure 9. Ring numbers 1 and 5 are rigidly attached to the inner and outer cylinders respectively. Ring numbers 2,3, and 4 are isolated from metal-to-metal contach by gas films. These rings should and take up intermediate rotation speeds between Ω_1 and Ω_2. Part number 6 provides a gas lubricated thrust bearing surface that balances the weight of the outer cylinder. These bearings resemble a plain journal bearing in that the bearing load is carried by high pressure gas in the shallow pockets embedded into precisely machined rings. Each ring bearing will have at least three of these pockets recessed into its surface and equally spaced around around the circumference. Each pocket is supplied with gas through its own calibrated orifice built into the ring and connected to a common source. When the outer cylinder is displaced from from its central position, some pockets have their outlets restricted, while diagonally opposite pockets are less restricted. The result is a differential pressure distribution that provides a restoring force to keep the system centered. In actual bearings the clearances are extremely small compared to those in normal bearings. In fact, it is standard practice for the journal to be a slight interference fit in the bearing when

idle. The required running clearance is provided by the expansion of the bearing when subjected to the internal pressure of the lubricating gas. Consequently, the system must be designed to never be rotated without the lubricating gas turned on. Since the gas viscosity is small compared to that for a liquid lubricant, there is no significant heat generated and thus no objection to ultra-tight clearances.

In this particular illustration, a five ring bearing system is shown. The high pressure lubricating gas, which also serves as the test medium, circulates through the channels in the bearing rings, fed by radial channels from the central axle. The entire assembly, including the outer cylinder, is supported by a thrust bearing (part number 6). The gas pressure in the annulus is held at a fixed increment above the outside pressure by a calibrated resistive element located in the outer cylinder (not shown). The development of such a system will require an extensive amount of engineering design and development. The allowable tolerances may be unattainable with present precision milling techniques. However, the experience gained during the completion of a phase I experiment may stimulate new ideas for implementing a phase II experiment.

CONCLUSIONS AND RECCOMMENDATIONS

An approach to constucting expermental apparati to validate the predicted behavior of acoustic wave propagation in the presence of strong pressure and temperature gradients has been described. The pressure and temperature gradient effects are directly manifested in the wave equation as a wavenumber shift proportional to the product of the two gradients. Experimentally, these effects can be measured as resonant frequency shifts and mode shape changes in a closed annular region between two co-rotating cylinders subjected to a radial temperature gradient. The pressure gradient can be controlled by varying the rotational speed. The temperature gradient would be controlled by differential heating of the two cylinders by electromagnetic induction. Differential heating is implemented by choosing a ferromagnetic alloy for the hot cylinder and a nonferromagnetic material for the cool cylinder. A constant temperature for the cool cylinder can be attained via evaporative cooling. Such a phase I experiment appears technically feasible with current technology.

Also, the feasibility of a phase II experiment is discussed. In this type experiment a dynamically stable, intense flow gradient is created in the annulus along with temperature and pressure gradients. The flow gradients can be introduced by decoupling the two rotating cylinders and providing them with independent drives. To simulate supersonic boundary layer flow and pressure gradients of interest, and stay within mechanical stress limits of availabe materials, the apparatus diameter should not be greater than about 1 meter and the test medium should be a low density, high molecular weight gas such as sulphur hexaflouride.

An additional complicating feature in a phase II experiment is the axial-boundary-condition perturbing effect on the flow profile. One possible mechanism for reducing this effect is to use a multiple concentric-ring bearing system to support the outer cylinder with respect to the inner cylinder. In principle, such a system should allow a linear Couette-type flow profile to be approximated. In actual fact however, current technology may not be able to produce such a system.

The successful completion of a phase I experiment should provide encouragement for the continued development of a long range experimental program to understand the combined effects of strong pressure, temperature and flow gradients on acoustic propagation in boundary layers. The experience gained in a phase I experiment and continued technology development may allow the impementation of a phase II experiment.

REFERENCES

1. Chandrasekhar, S.: Hydrodynamics and Hydromagnetic Stability. Oxford University Press, 1961. Also by Dover Publications, Inc., 1981.

2. Di Prima, R. C.; and Swinney, H. L.: *Instabilities and Transition in Flow Between Concentric Rotating Cylinders.* Topics in Applied Physics, Vol. 45—Hydrodynamic Instabilities and the Transition to Turbulence. H. L. Swinney and J. P. Golub, Editors. Springer-Verlag, New York, 1981.

3. Taylor, G. I.: Stability of a Viscous Liquid contained between Two Rotating Cylinders, Phil. Trans. of the Royal Soc. of London, Series A, Vol. 223, 1923, pp. 289-343.

4. Coles, D.: Transition in circular Couette flow. J. Fluid Mech., Vol. 21, 1965, pp. 385-425.

5. Andereck, C. D.: Liu, S. S.; and Swinney, H. L.: Flow regimes in a circular Couette system with independent rotating cylinders. J. Fluid Mech., Vol. 164, 1986, pp. 155-183.

7. Wimmer, M.: Experiments on the stability of viscous flow between two concentric rotating spheres. J. Fluid Mech., Vol. 103, 1981, pp. 117-131.

8. Zorumski, William E.: Acoustic Response of a Rectangular Waveguide with a Strong Transverse Temperature Gradient. NASA TM-101564, March, 1989.

9. Zorumski, William E.: Acoustic Waves in Gases with Strong Pressure Gradients. AIAA paper 89-1087, April, 1989.

10. Gans, Roger F.: On the Poincare problem for a compressible medium. J. Fluid Mech., Vol. 62, part 4, 1974, pp. 637–675.

11. Koutsoyannis, S. P.: Characterization of Acoustic Disturbances in Linearly Sheared Flows. J. Sound Vib., Vol. 68, No. 2. January, 1980, pp. 187–202.

12. Coles, D.; and Van Atta, C.: Measured Distortion of a Laminar Circular Couette Flow by End Effects. J. Fluid Mech., Vol. 25, part 3, 1966, pp. 513–521.

13. Stanley, J.K.: Electrical and Magenetic Properties of Metals. American Society for Metals, Metals Park, Ohio, 1963.

14. Simpson, P.G.: Induction Heating, Coil and System Design. McGraw Hill, N.Y. 1950.

15. Whitley, S.: Review of the gas centrifuge until 1962. Part II: Principles of high-speed rotation. Reviews of Modern Physics, Vol. 56, 1984, pp. 67-97.

16. Fuller, D.D.: Theory and Practice of Lubrication for Engineers, 2nd ed. John Wiley and Sons, 1984.

TABLE I

MATERIALS OF INTEREST FOR ROTATINC CYLINDER APPARATUS

Material	Density	Yield Stress	Melt Temp	Curie Temp	Rel Mag Perm
	kg/m^3	N/m^2	°C	°C	
[a]Aluminum	2740	$4.7 \cdot 10^8$	480		1
[a]Steel	7850	$3.3 \cdot 10^8$	1500	(720)	(5000)
[b]UHSsteel	7800	$19.0 \cdot 10^8$	(1500)	(720)	(5000)
[a]Titanium	4850	$13.1 \cdot 10^8$	1700	1700	1
[b]Supermendur	8200			980	66000

a) Marks Handbook for Mechanical Engineers. 7th ed, (6-10)
b) Stanley, J. K.: Electrical Properties of Metals. p 268
( ) denotes estimates based on similar material

TABLE II

FLUIDS OF INTEREST FOR ROTATING CYLINDER APPARATUS

Gas/ Liquid	Density	Thermal Cond	Specific Heat	Viscosity	Sound Speed	Gas Const	γ
	kg/m^3	$W/m \cdot K$	$J/kg \cdot K$	$N \cdot s/m^2$	m/s	$m^2/s^2 \cdot K$	c_p/c_v
Air	[a]1.21	$2.47 \cdot 10^{-2}$	[a]1009	$[a]1.81 \cdot 10^{-5}$	[a]343	287	1.402
SF_6	[a]6.16	$1.41 \cdot 10^{-2}$	[b]665	$[c]1.56 \cdot 10^{-5}$	136	56.9	1.1105
CCl_2F_2	5.17			$1.25 \cdot 10^{-5}$	150	68.7	1.130
H_2O	[a]998	0.61	4189	$1.00 \cdot 10^{-3}$			

a) 20°C; b) 25°C; c) 30°C

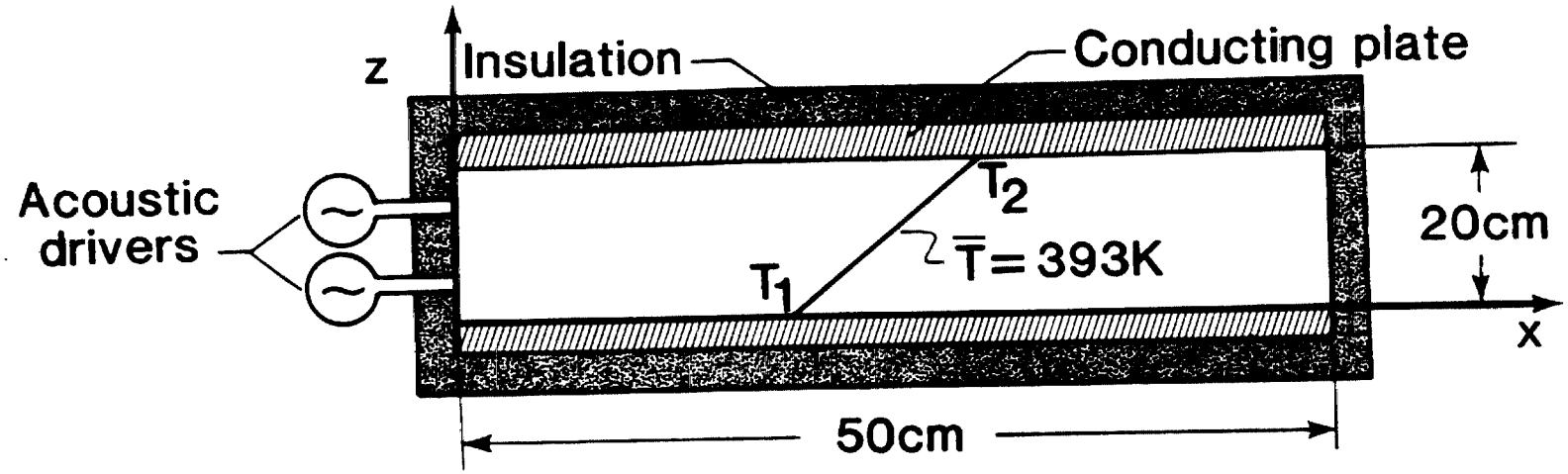

(a) Waveguide with transverse temperature gradient

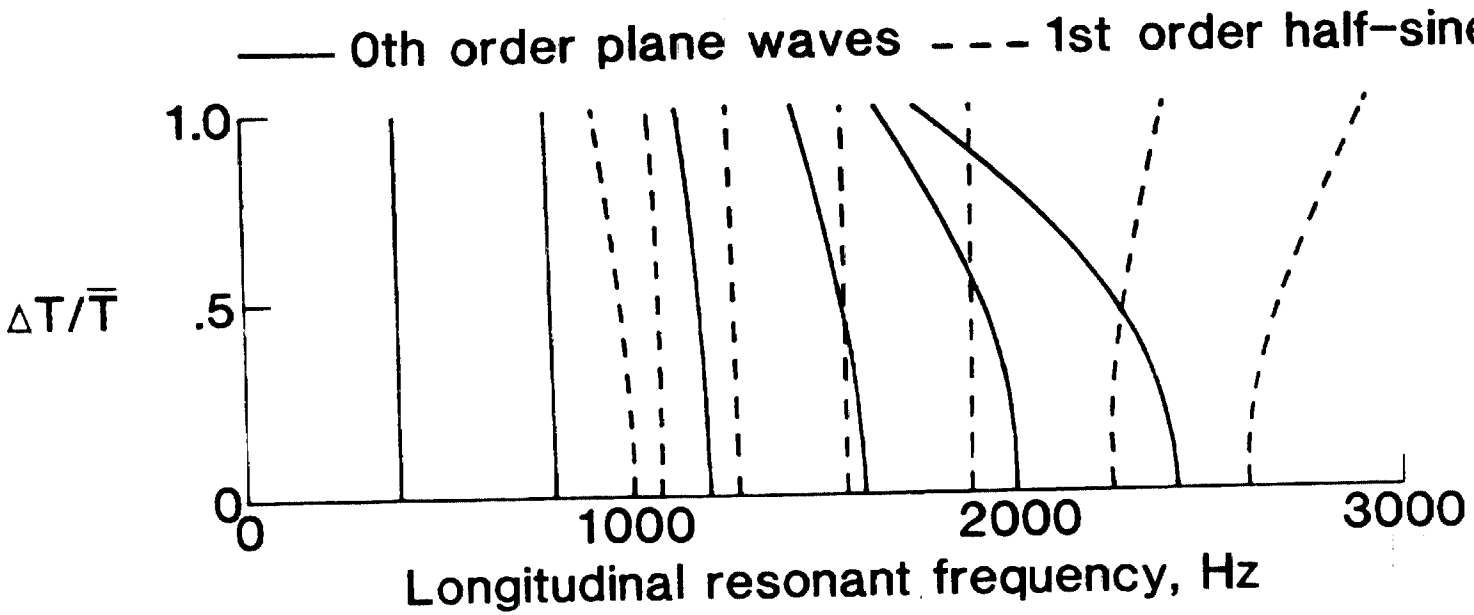

(b) Resonant frequency shift induced by temperature gradient

Figure 1. Strong temperature gradient effects in acoustic transmission.

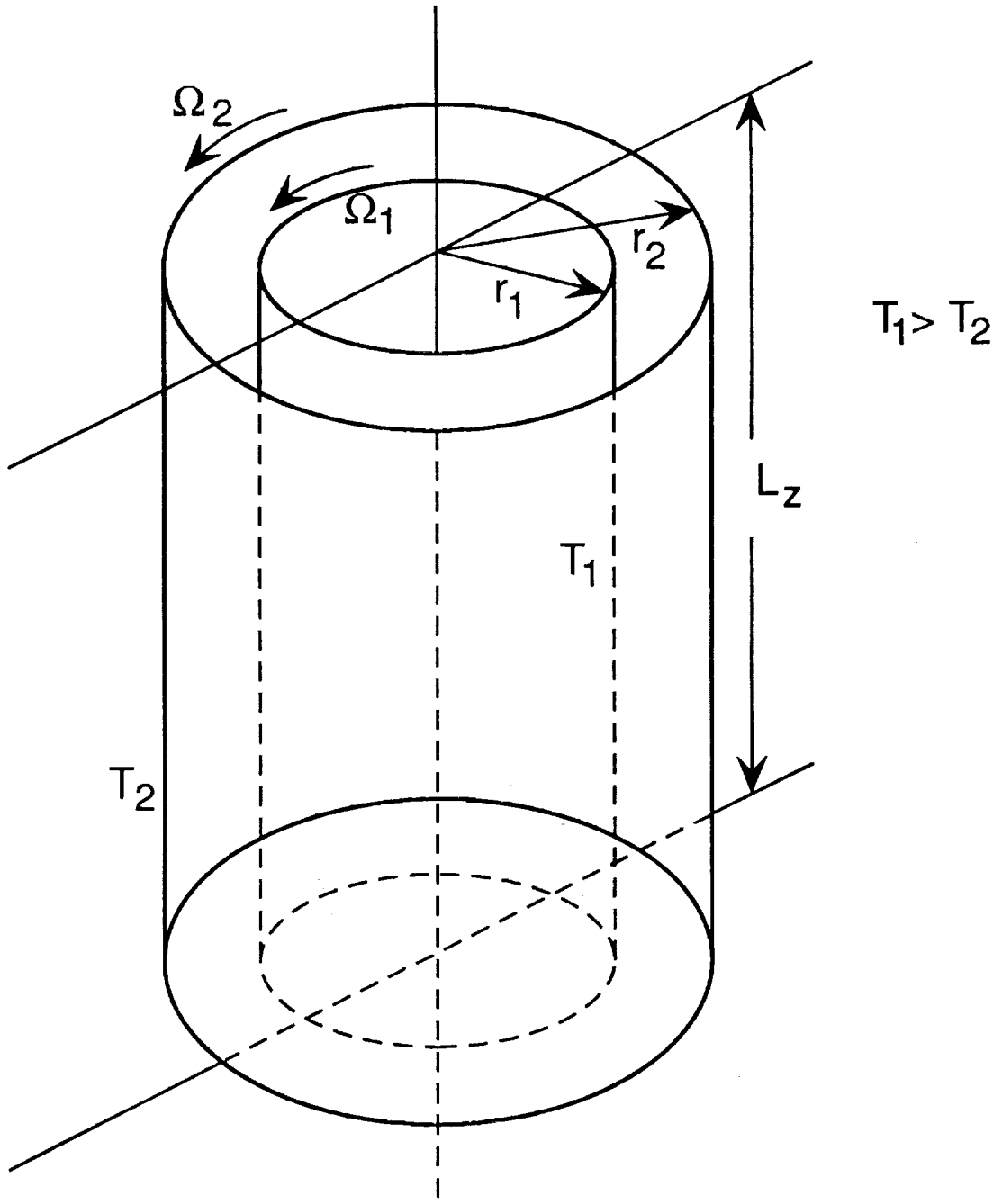

Figure 2. Rotating cylinder apparatus. $\Omega_1 = \Omega_2$ for Phase 1, Ω_1, Ω_2 independently controlled for Phase II.

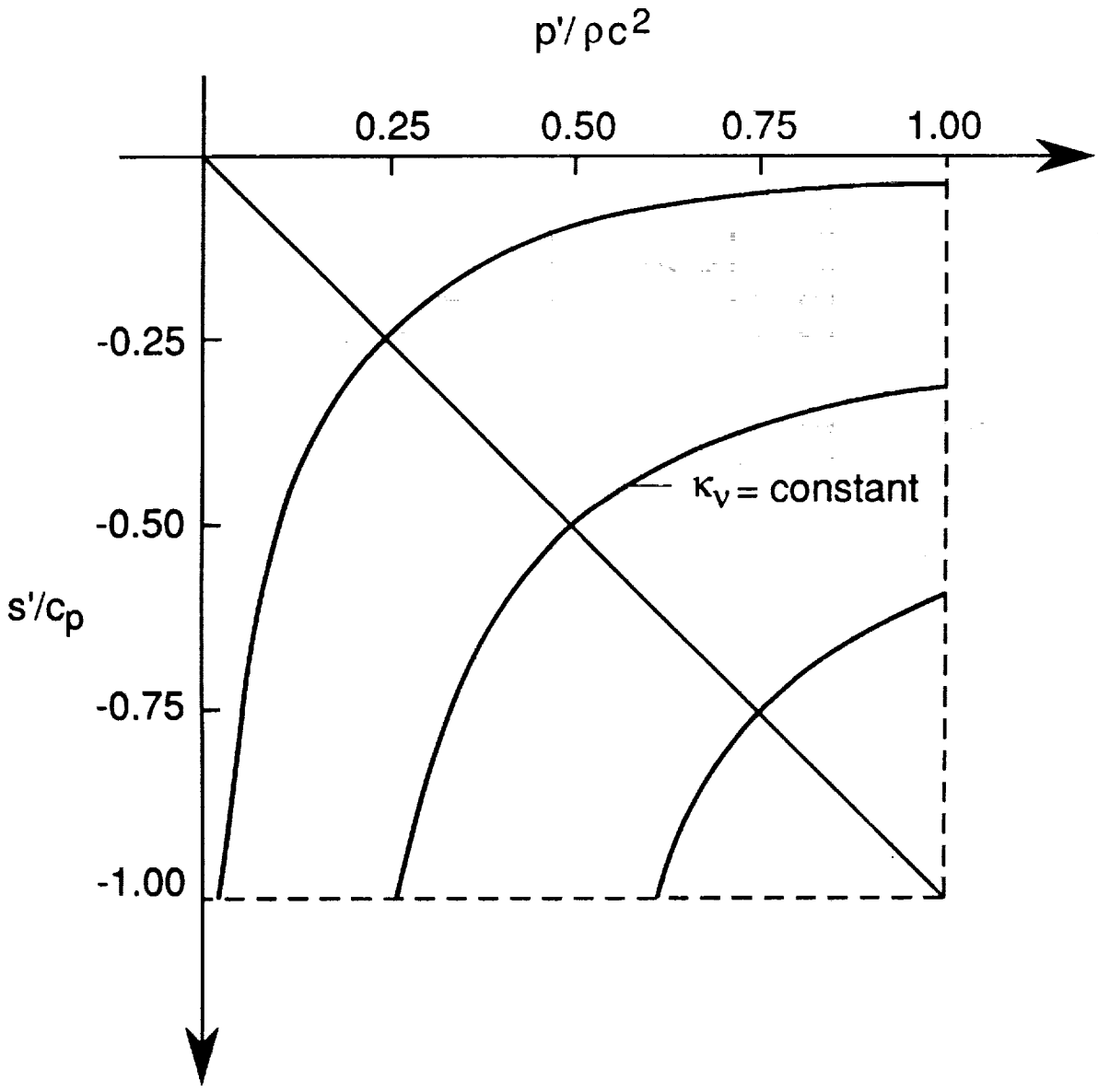

Figure 3. Range of pressure and entropy gradient for Phase I experiment.

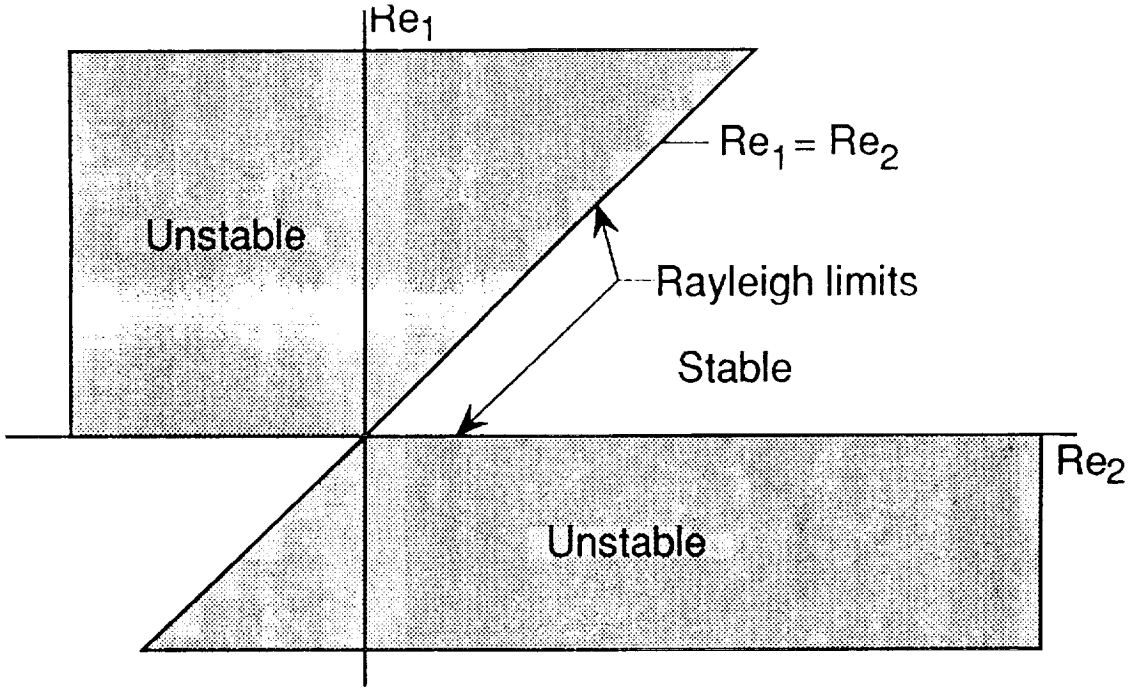

a. inviscid limits- arbitrary scale

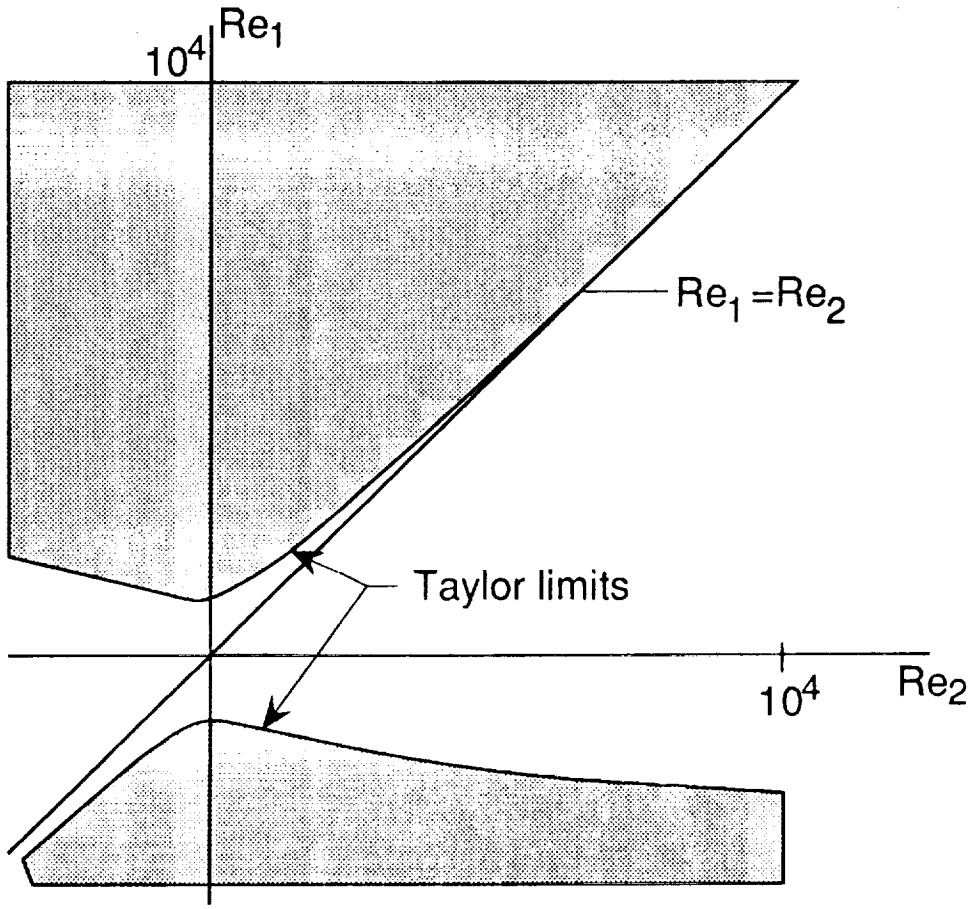

b. viscous limits on 10^4 scale

Figure 4. Stability limits for incompressible Couette flow. Graphs are not accurate and are intended to show qualities only.

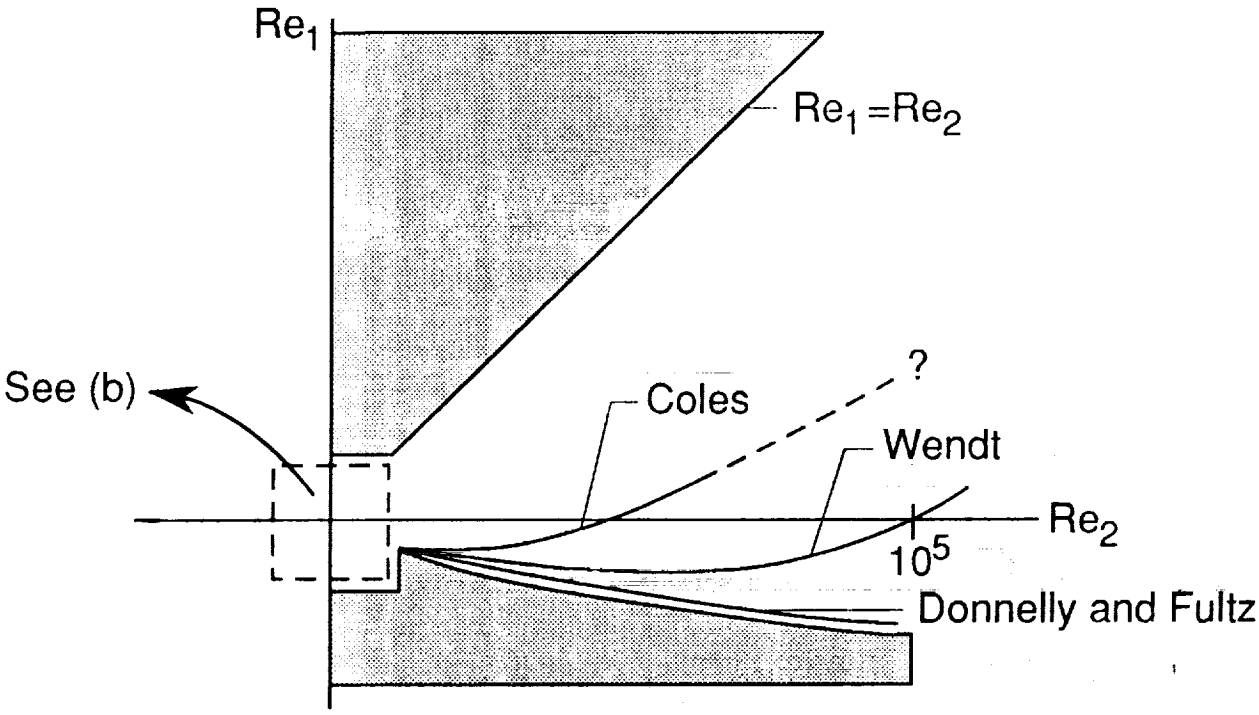

c. viscous limits on 10^5 scale

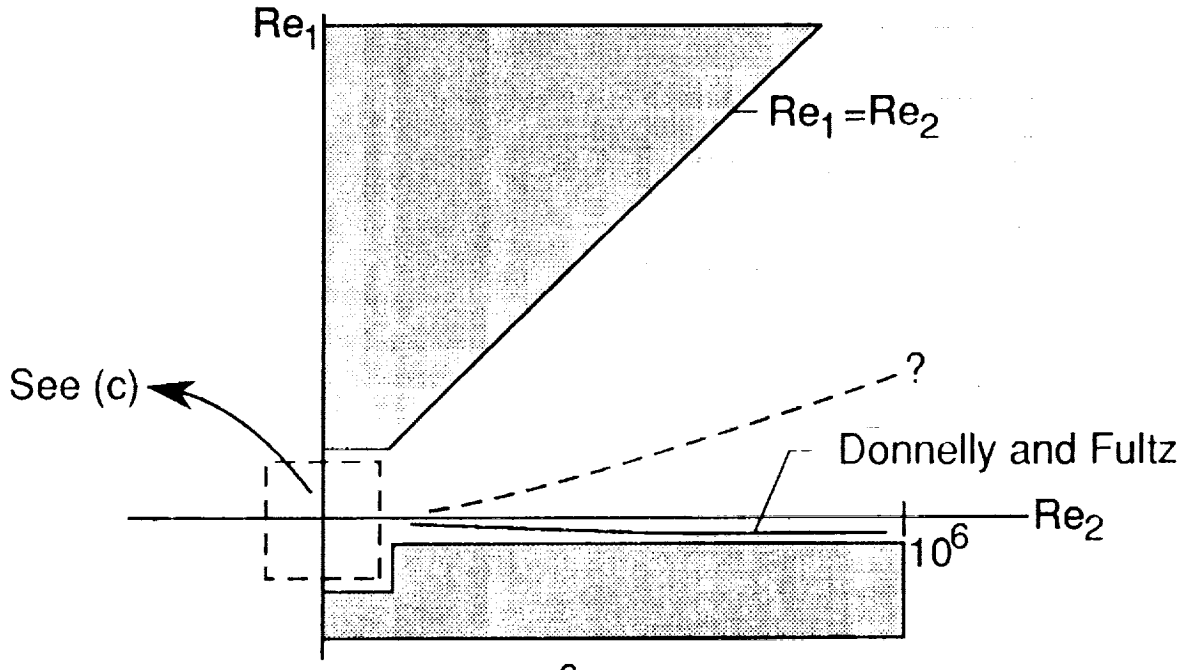

d. viscous limits on 10^6 scale

Figure 4. Completed

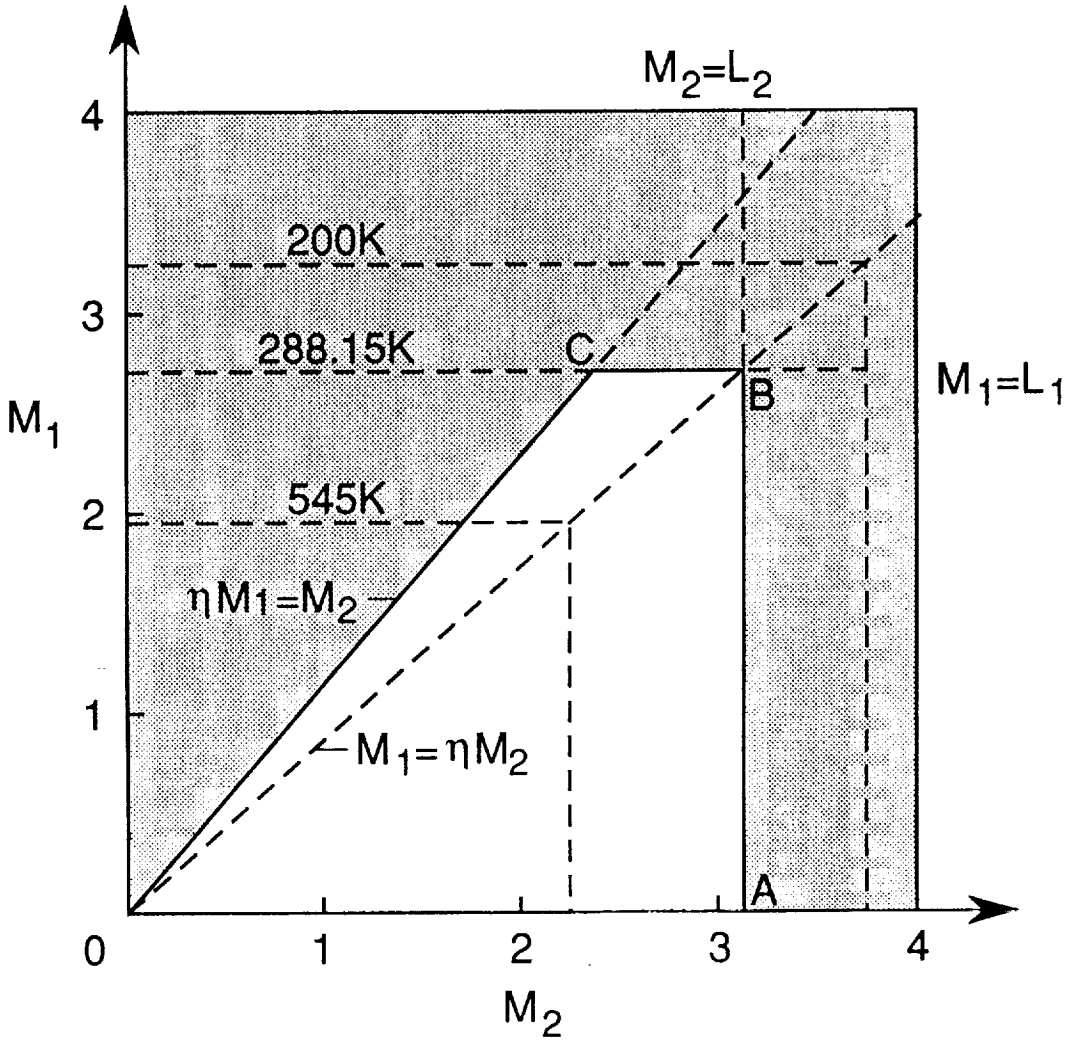

Figure 5. Mach number range for Phase II apparatus using Sulphur Hexaflouride, constant temperature.

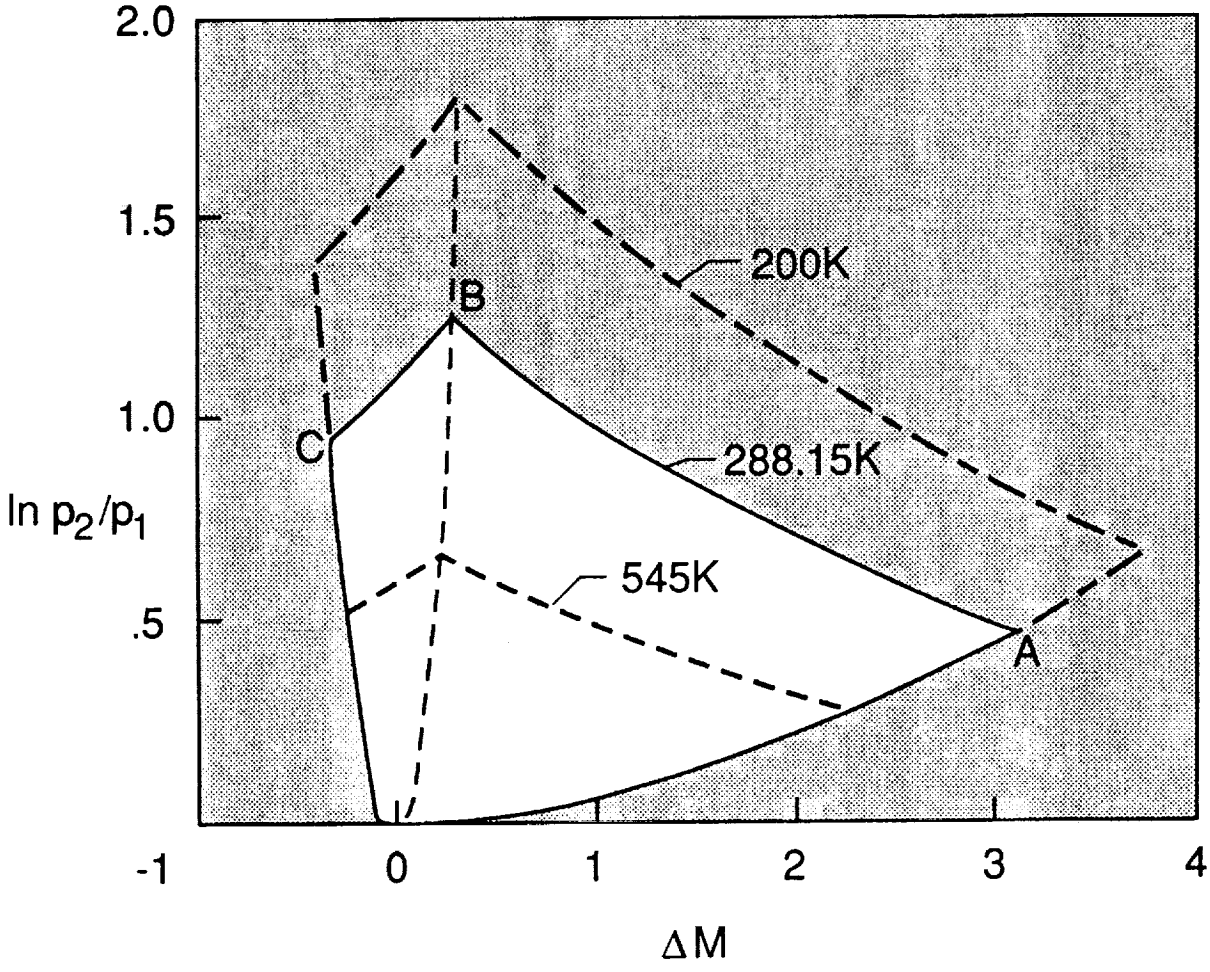

Figure 6. Range of relative Mach number and pressure ratio for Phase II apparatus using Sulphur Hexaflouride, constant temperature.

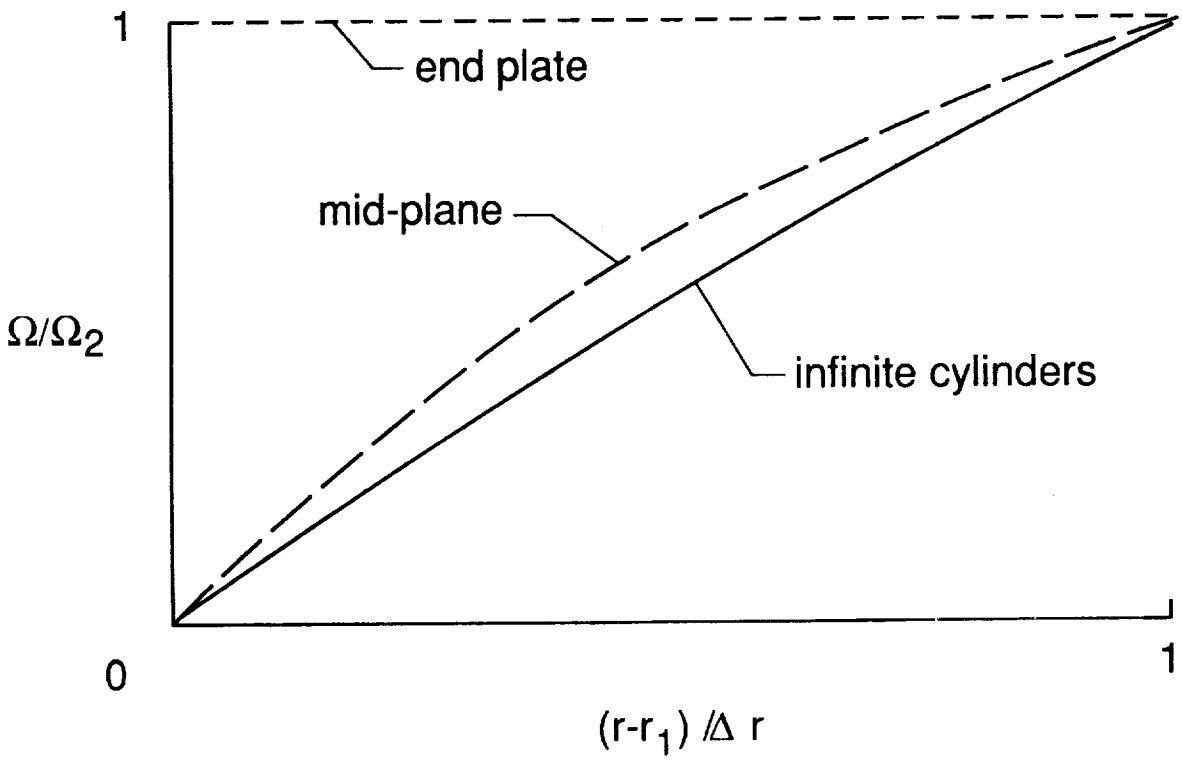

Figure 7. Effect of end plates on angular velocity between rotating cylinders-inner cylinder fixed.

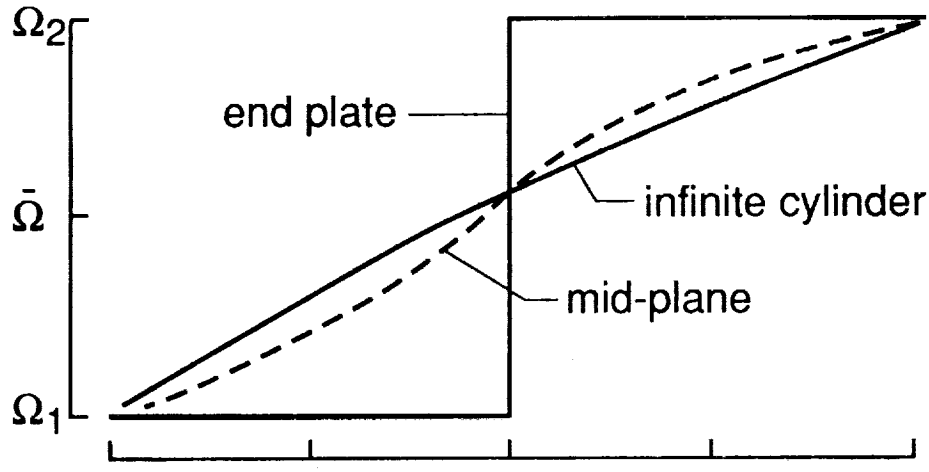

a. divided end plate

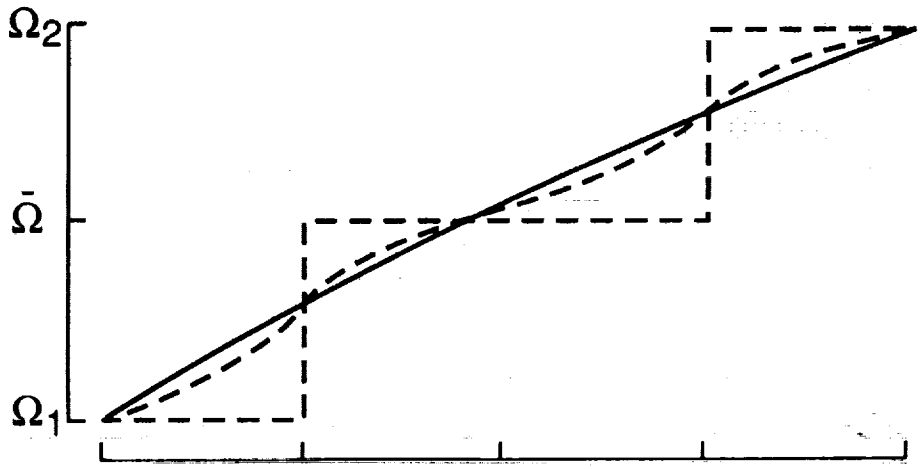

b. end plate with central segment

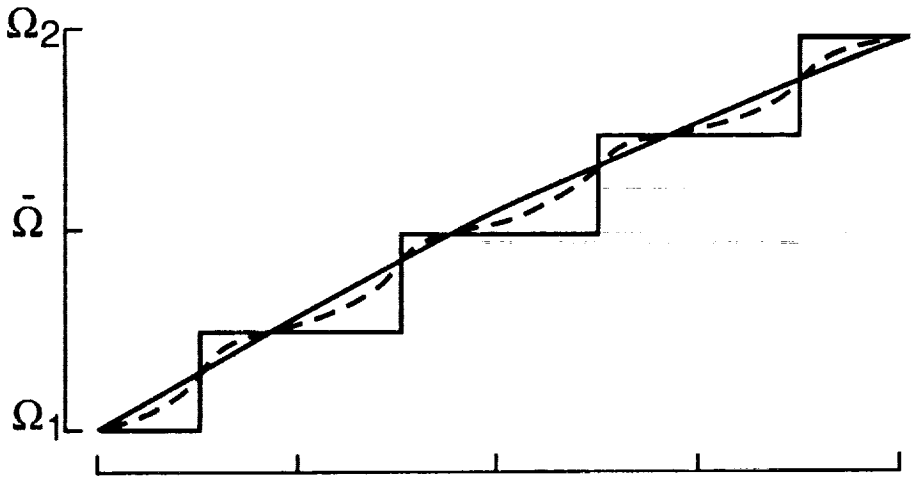

c. multi-segment end plate

Figure 8. Cylinder end angular velocity profiles with segmented end plates.

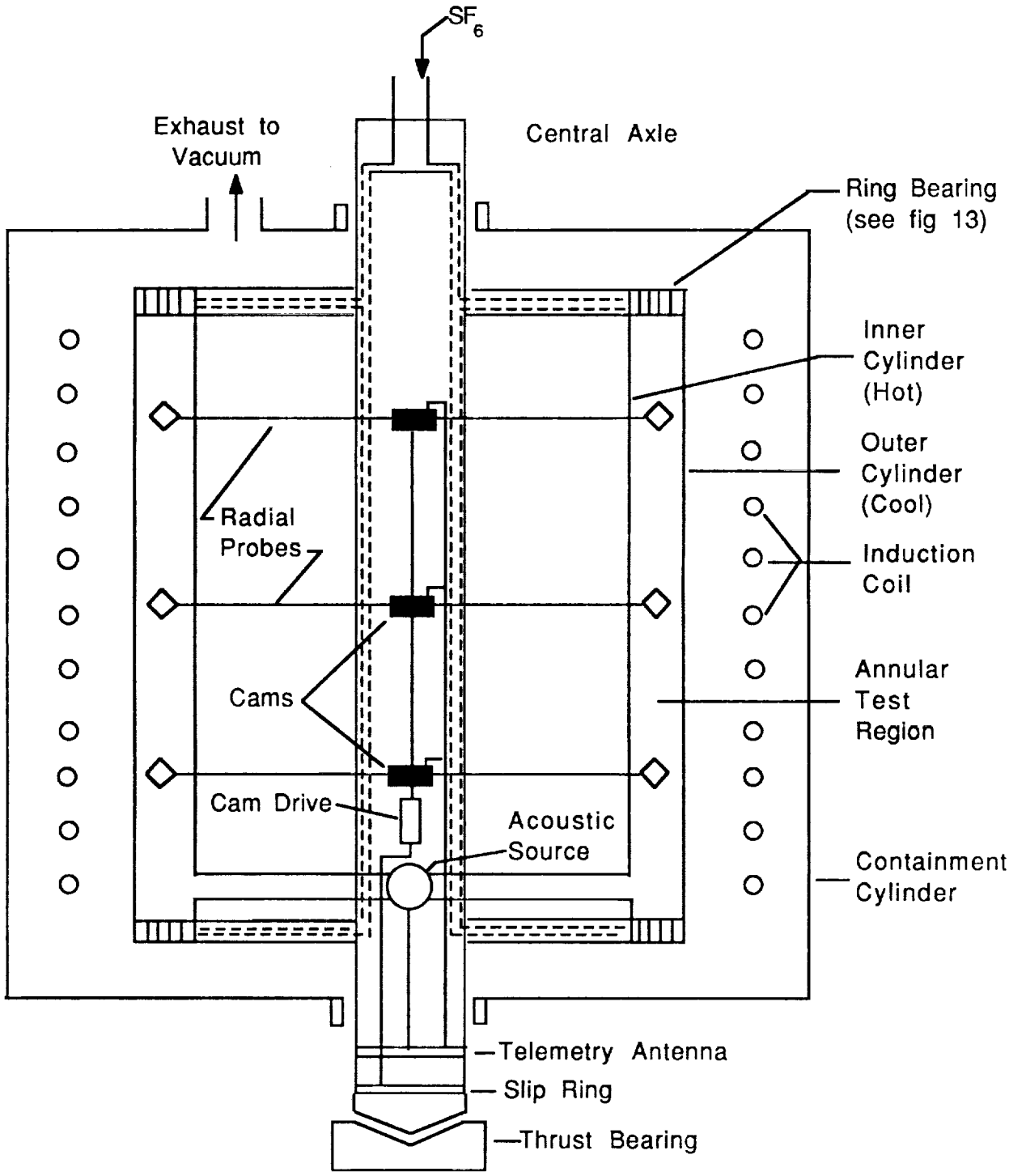

Figure 9 Cross section sketch of phase II experimental apparatus concept.

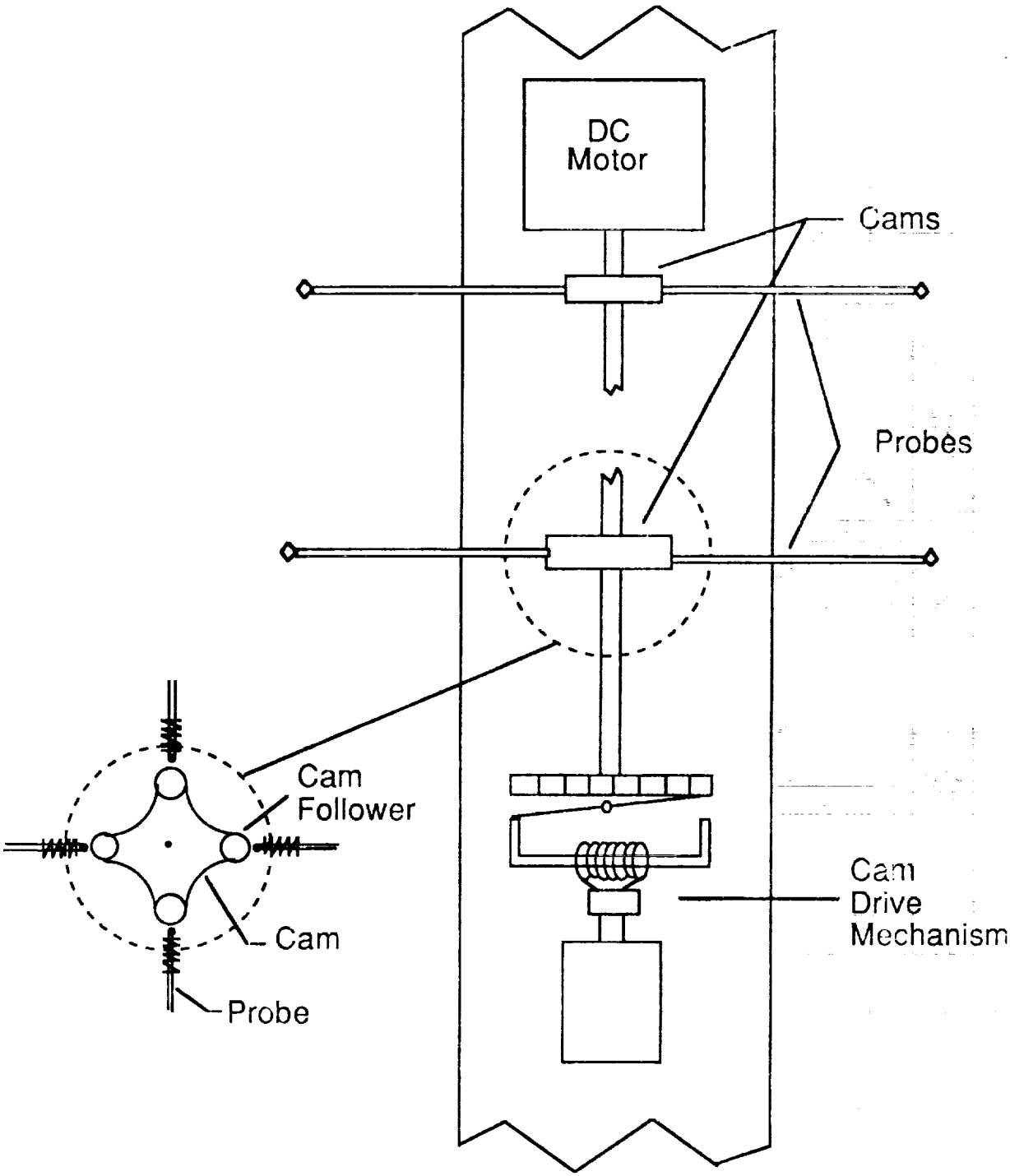

Figure 10. Schematic of multi-probe traversing system.

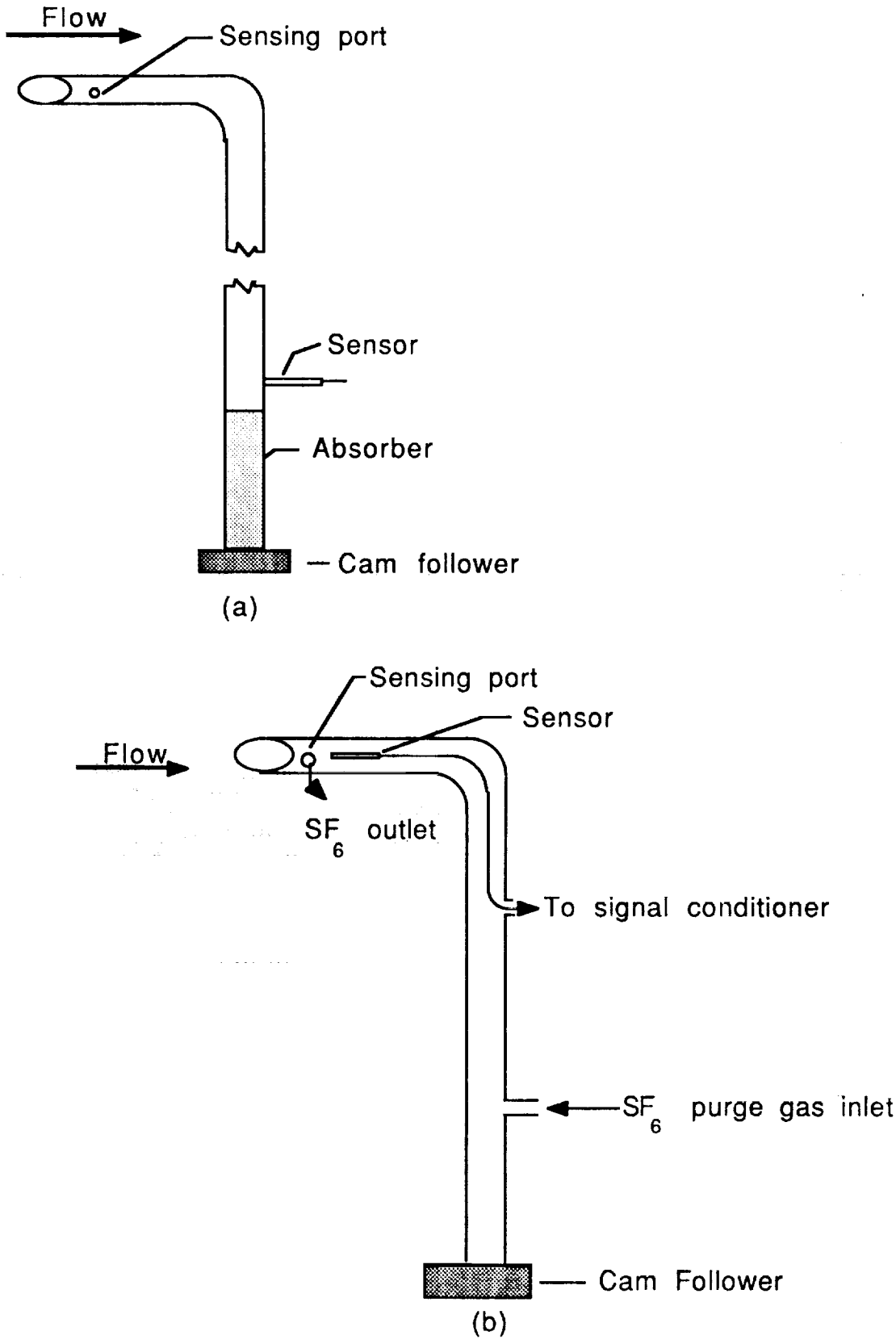

Figure 11. Radial probe design concept for annulus.

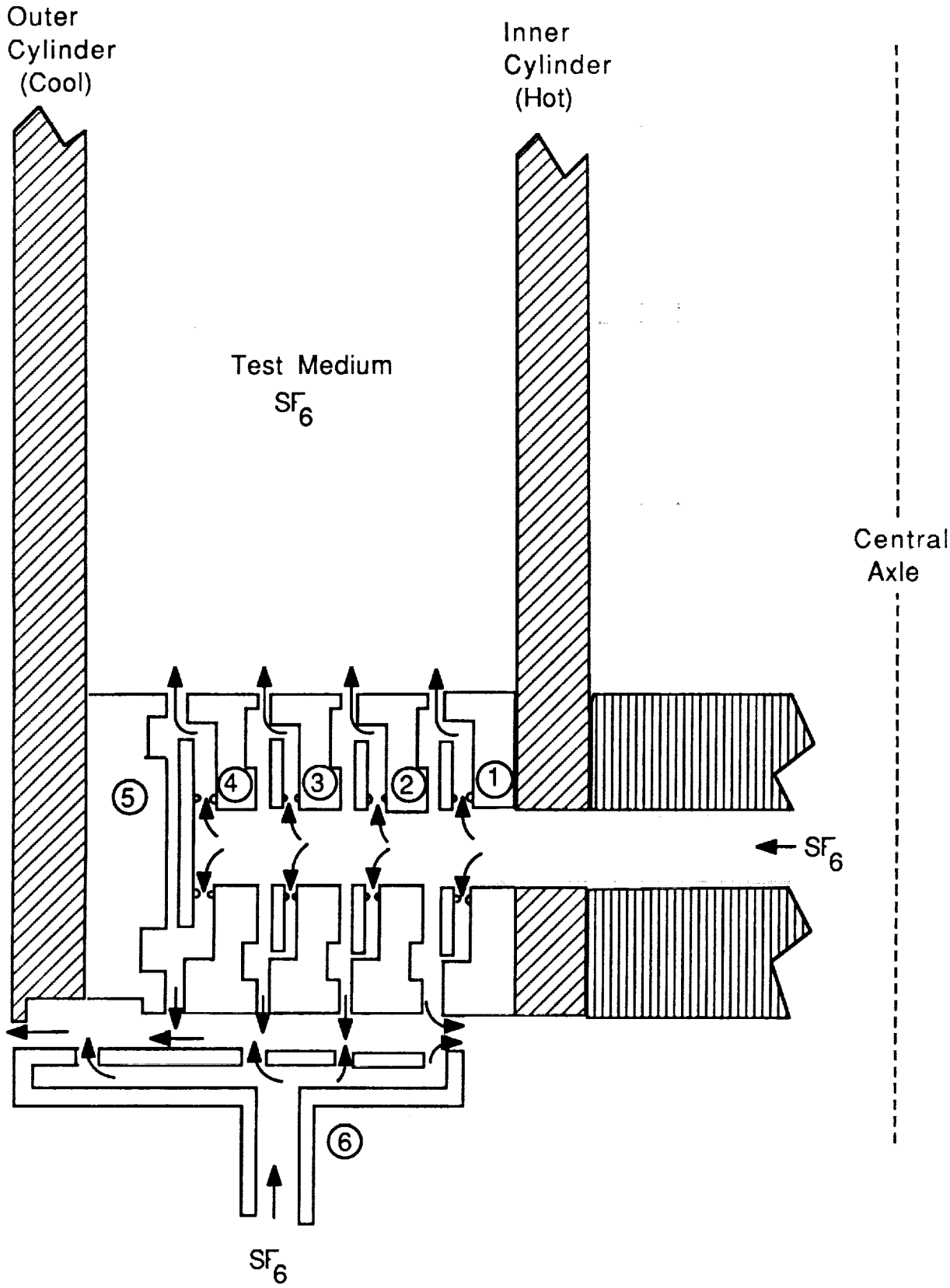

Fig 12. Design concept for gas lubricated, multi-ring bearing for outer cylinder.

NASA
National Aeronautics and Space Administration

Report Documentation Page

1. Report No.	2. Government Accession No.	3. Recipient's Catalog No.
NASA TM-102621		

4. Title and Subtitle
Experimental Feasibility of Investigating Acoustic Waves in Couette Flow with Entropy and Pressure Gradients

5. Report Date
February 1990

6. Performing Organization Code

7. Author(s)
Tony L. Parrott, William E. Zorumski, and John W. Rawls, Jr.*

8. Performing Organization Report No.

10. Work Unit No.
763-01-41-27

9. Performing Organization Name and Address
NASA Langley Research Center
Hampton, VA 23665-5225

11. Contract or Grant No.

13. Type of Report and Period Covered
Technical Memorandum

12. Sponsoring Agency Name and Address
National Aeronautics and Space Administration
Washington, DC 20546-0001

14. Sponsoring Agency Code

15. Supplementary Notes
*Lockheed Engineering & Sciences Corporation
Hampton, VA

16. Abstract

This paper discusses the feasibility of an experimental program for studying the behavior of acoustic wave propagation in the presence of strong gradients of pressure, temperature, and flow. Theory suggests that gradients effects can be experimentally observed as resonant frequency shifts and mode shape changes in a waveguide. A convenient experimental geometry for such experiments is the annular region between two co-rotating cylinders.

Radial temperature gradients in a spinning annulus can be generated by differentially heating the two cylinders via electromagnetic induction. Radial pressure gradients can be controlled by varying the cylinder spin rates. Present technology appears adequate to construct an apparatus to allow independent control of temperature and pressure gradients.

A complicating feature of a more advanced experiment, involving flow gradients, is the requirement for independently controlled cylinder spin rates. Also, the boundary condition at annulus terminations must be such that flow gradients are minimally disturbed. The design and construction of an advanced apparatus to include flow gradients will require additional technology development.

17. Key Words (Suggested by Author(s))	18. Distribution Statement
Couette flow Acoustic waves Pressure gradients Entropy gradients	Unclassified - Unlimited Subject Category 71

19. Security Classif. (of this report)	20. Security Classif. (of this page)	21. No. of pages	22. Price
Unclassified	Unclassified	51	A04